KAUNAS UNIVERSITY OF TECHNOLOGY
FACULTY OF MATHEMATICS AND NATURAL SCIENCES

Marijus Astrauskas

OPTIMISATION OF LOW DOSE COMPUTED TOMOGRAPHY PROTOCOL FOR DIAGNOSTICS OF DEVELOPMENTAL DYSPLASIA OF THE HIP USING A PHANTOM BASED NOISE SIMULATION APPROACH

Final Master Degree Project

Supervisor
Prof. dr. Diana Adlienė (KTU)

Consultant
Dr. Jonas Venius (National Cancer Institute, Lithuania)

KAUNAS, 2017

KAUNAS UNIVERSITY OF TECHNOLOGY
FACULTY OF MATHEMATICS AND NATURAL SCIENCES

OPTIMISATION OF LOW DOSE COMPUTED TOMOGRAPHY PROTOCOL FOR DIAGNOSTICS OF DEVELOPMENTAL DYSPLASIA OF THE HIP USING A PHANTOM BASED NOISE SIMULATION APPROACH

Final Master Degree Project
Medical Physics (code 621B92002)

Supervisor
Prof. dr. Diana Adlienė

Consultant
Dr. Jonas Venius

Reviewer
Doc. dr. Leonas Jakevičius

Project prepared by
Marijus Astrauskas

KAUNAS, 2017

KAUNO TECHNOLOGIJOS UNIVERSITETAS

(Fakultetas)

(Studento vardas, pavardė)

(Studijų programos pavadinimas, kodas)

"OPTIMISATION OF LOW DOSE COMPUTED TOMOGRAPHY PROTOCOL FOR DIAGNOSTICS OF DEVELOPMENTAL DYSPLASIA OF THE HIP USING A PHANTOM BASED NOISE SIMULATION APPROACH"

AKADEMINIO SĄŽININGUMO DEKLARACIJA

___ . _____ ____ .
Kaunas

Patvirtinu, kad mano, **Marijaus Astrausko**, baigiamasis projektas tema „**Optimisation of low dose computed tomography protocol for diagnostics of developmental dysplasia of the hip using a phantom based noise simulation approach**", yra parašytas visiškai savarankiškai ir visi pateikti duomenys ar tyrimų rezultatai yra teisingi ir gauti sąžiningai. Šiame darbe nei viena dalis nėra plagijuota nuo jokių spausdintinių ar internetinių šaltinių, visos kitų šaltinių tiesioginės ir netiesioginės citatos nurodytos literatūros nuorodose. Įstatymų nenumatytų piniginių sumų už šį darbą niekam nesu mokėjęs.

Aš suprantu, kad išaiškėjus nesąžiningumo faktui, man bus taikomos nuobaudos, remiantis Kauno technologijos universitete galiojančia tvarka.

_____ _____

(vardą ir pavardę įrašyti ranka) *(parašas)*

Marijus, Astrauskas. Optimisation of low dose computed tomography protocol for diagnostics of developmental dysplasia of the hip using a phantom based noise simulation approach. Master's Final Project / supervisor prof. dr. Diana Adlienė (KTU), consultant dr. Jonas Venius (NCI); Faculty of Mathematics and Natural Sciences, Kaunas University of Technology.

Research field and area: Medicine and Health, Biomedical Sciences.

Keywords: computed tomography, low dose protocol, developmental dysplasia of the hip, noise simulation.

Kaunas, 2017. 50 p.

SUMMARY

There is a number of different diagnostic imaging modalities used for diagnostics and postoperative control of developmental dysplasia of the hip (DDH). One of them is computed tomography (CT). It is the main imaging method for older pediatric patients – 6 months or older, because their pelvic and femoral bone structures begin to ossify, making ultrasound less informative. Simple radiography is also not informative enough, especially when there is a need for postoperative control, when the child is in a spica cast. Considering, that in pediatrics there is high demand for low dose protocols, the goal of this thesis was to approve the possibility for a significant reduction of CT examination doses to the pediatric patients, suffering from DDH. This was implemented using a phantom based noise simulation approach.

The investigation was performed in Vilnius University Hospital Santaros Klinikos Children's Hospital, using the CT scanner "Siemens Somatom Sensation 64" and in collaboration with local radiologists. During the study, a noise simulation algorithm was constructed, which uses generated noise samples obtained from CT scans made using the phantom measurements performed at different mAs (tube current and exposure time scanning parameter). These noise samples indicated the amount of noise that was present in the CT image when it was scanned using specific parameters. The noise samples were combined with the original patient images obtained using various scanning parameters and the end-result was an image with a noise level at the selected scan parameter.

Using the created noise simulation algorithm, the image sets from 20 patients were simulated for 13, 20 and 50 mAs scans. Simulated image sets were revised and evaluated by the radiologist from Santaros Klinikos Children's Hospital. There were 6 evaluation criteria selected, with a 3 point scale for quality: 1 - poor visibility of structures, 2 – acceptable visibility, 3 – good visibility. The results were differentiated into two outcome groups: 1 point – negative outcome, 2 or 3 points – positive outcome. After analyzing the results from the evaluations it was found that

there were no negative outcomes for the 50 mAs and 20 mAs simulations. For 13 mAs simulations there were only 3 negative outcomes that were not critical for the control of the pathology and they represented 2.51% from overall evaluations.

Based on these evaluation results it was concluded, that the images scanned using 13 mAs are of an acceptable quality for successful clinical evaluation and postoperative control of the DDH case. An optimized low dose CT protocol was recommended for examination of pediatric patients having developmental dysplasia of the hip. After analysing the scan data of the original patients, it was found that if these patients were scanned with the suggested low dose CT protocol, their dose, on average, would have been significantly reduced - by a factor of 6.7±3.8.

Marijus, Astrauskas. Mažų dozių kompiuterinės tomografijos protokolo optimizavimas įgimto klubo sąnario iškrypimui tirti naudojant triukšmų modeliavimą. Magistro baigiamasis projektas / vadovė prof. dr. Diana Adlienė (KTU), konsultantas dr. Jonas Venius (NVI); Kauno technologijos universitetas, matematikos ir gamtos mokslų fakultetas.

Mokslo kryptis ir sritis: Medicina ir sveikata, Biomedicinos mokslai.

Reikšminiai žodžiai: kompiuterinė tomografija, mažų dozių protokolas, klubo sąnario deformacija, triukšmo modeliavimas.

Kaunas, 2017. 50 p.

SANTRAUKA

Įgimtos klubų sąnario deformacijos patologijos ištyrimui gali būti naudojami įvairūs diagnostiniai metodai. Vienas iš jų – kompiuterinės tomografijos (KT) tyrimas. Šis metodas dažniausiai yra pradedamas taikyti vaikams, nuo šeštojo mėnesio, kuomet pradeda kaulėti arba jau yra pilnai sukaulėjusios klubo sąnario ir šlaunikaulio struktūros, kurių nebeįmanoma įvertinti naudojant kitus diagnostinius metodus, tokius kaip ultragarsas ar paprasta radiografija. Taip pat, atliekant šios patologijos korekciją, kūdikių klubai yra fiksuojami gipse, kas dar labiau komplikuoja įprastinės radiografijos taikymą. Kadangi pediatrijoje ypač aktyviai siekiama sumažinti gaunamas dozes radiologinių procedūrų metu, šio tyrimo metu buvo siekiama įrodyti, jog kliniškai teisingą įvertinimą tiek pooperacinės kontrolės, tiek pakartotinių apžiūrų metu, galima atlikti su ženkliai mažesniais KT skenavimo parametrais, taip sumažinant pacientams tenkančią apšvitą.

Tyrimas buvo atliktas VšĮ VUL Santaros Klinikų vaikų ligoninėje, naudojant kompiuterinį tomografą “Siemens Somatom Sensation 64” ir bendradarbiaujant su gydytojais radiologais. Visi tyrimui naudoti vaizdai buvo gauti skenuojant su tuo pačiu KT aparatu. Tyrimo metu buvo sukurtas triukšmo simuliacijos algoritmas, kuriame naudojamos triukšmo bazės gaunamos iš KT skenuojamo fantomo. Siekiant nustatyti triukšmo lygį prie tam tikrų skenavimo parametrų ir suformuoti teisingas triukšmo bazes, buvo sukonstruotas želatinos fantomas, kurio suminis slopinimo koeficientas artimas vandens (HU-10). Nuskenavus šį fantomą buvo sugeneruotos specialios “triukšmo bazės”, kurios atitinka triukšmo lygį, atsirandantį skenuojant pasirinktais parametrais. Šios bazės buvo modifikuojamos ir pridedamos prie originalių pacientų vaizdų, siekiant išgauti simuliuotus vaizdus, kuriuose triukšmas atitiktų mažų parametrų/dozių skenavimus. Siekiant teisingai modifikuoti triukšmo bazes, buvo įvertinta paciento dydžio, skenavimo parametrų, gipso įtaka vaizdo triukšmui ir simuliacijos algoritmas buvo atitinkamai pritaikytas atsižvelgiant į rezultatus.

Naudojant simuliacijos algoritmą buvo sugeneruoti 20 pacientų vaizdai, kuriuose triukšmo lygis atitiktų vaizdų, gautų skenuojant prie 13, 20, 50 mAs (srovės stiprio ir ekspozicijos laiko) triukšmų lygį. Simuliuoti vaizdai įvertinimui buvo perduoti VšĮ VUL Santariškių klinikų gydytojai radiologei. Gydytoja pagal 6 kriterijus vertino simuliuotų vaizdų 2D ir 3D rekonstrukcijas. 2D rekonstrukcijose vertinta: tinkamumas kampo matavimui, tinkamumas korekcijos įvertinimui, gūžduobės kaulų kraštų aštrumas, šlaunikaulio sukaulėjusio krašto aštrumas. 3D rekonstrukcijoje vertinta: šlaunikaulių pozicijos įvertinimas (matomumas) gūžduobės atžvilgiu, tinkamumas kampo matavimui. Vertinimas buvo atliktas naudojant 3 balų skalę: 3 balai - įvertinimas/matomumas geras, 2 balai - įvertinimas/matomumas priimtinas, 1 balas - įvertinimas/matomumas blogas. Sumuojant rezultatus, kriterijai įvertinti 2 arba 3 balais buvo laikomi teigiamais, surinkę 1 balą – neigiamais.

Vertinant vaizdus, atitinkančius 50 mAs skenavimą, buvo nustatyta, jog visų pacientų vaizduose buvo įmanomas tinkamas klinikinis patologijos įvertinimas ir pooperacinė kontrolė - 88.6% pacientų vaizdų buvo įvertinti gerai, 13.3% įvertinti kaip patenkinami, todėl visi vaizdai buvo įvertinti teigiamai. Vertinant vaizdus, atitinkančius 20 mAs skenavimą, taip pat nustatyta, jog visų pacientų vaizduose buvo įmanomas tinkamas klinikinis patologijos įvertinimas ir pooperacinė kontrolė - 88,33% pacientų vaizdų buvo įvertinti gerai, 11,66% įvertinta patenkinamai, todėl visi vaizdai buvo įvertinti teigiamai. Vertinant vaizdus, atitinkančius 13 mAs skenavimą, buvo nustatyta, jog kai kuriems parametrams įvertinti vaizdai buvo netinkami, tačiau esminius patologijos įvertinimus buvo įmanoma atlikti. 70,83% vaizdų buvo įvertinti kaip geri, 26,66% - patenkinami, o neigiamų įvertinimų buvo 2,51% (iš viso 3).

Išanalizavus vaizdų vertinimo rezultatus nustatyta, jog skenuojant pacientus 13 mAs, įmanomas kliniškai geras patologijos įvertinimas ir pooperacinė kontrolė. Remiantis šiais rezultatais, pasiūlytas naujas pediatrinis KT skenavimo protokolas skirtas įgimtos klubų deformacijos diagnostikai ir pooperacinei kontrolei, kuris leistų sumažinti pacientų gaunamą apšvitą 6.7±3.8 karto, lyginant su tyrimui naudotais pacientų skenavimo duomenimis.

LIST OF CONTENTS

LIST OF FIGURES

LIST OF TABLES

INTRODUCTION

Computed tomography (CT) is a widely used diagnostic imaging modality since it was introduced in 1970's. It can be used for a number of localizations and in various fields of medical diagnostics: oncology, orthopedics, neurology and many others. Since this method is using ionizing radiation there are some health risks associated with it and therefore it should be used in accordance with the ALARA (as low as reasonably achievable) principle, especially in pediatric diagnostics. Although a lot has been achieved during the past decade in optimizing various CT protocols for better image quality, optimizations for diagnostic accuracy that is dependent on the indications of the specific pathology cases is largely overlooked.

One of the protocols, that could potentially be optimized and is discussed, is devoted to the diagnostics, postoperative and follow-up control of developmental dysplasia of the hip (DDH). This pathology is usually caught early and can be diagnosed with various other imaging modalities during the early months of life, however after some time clinically reliable information can no longer be obtained without the use of ionizing radiation. By using computed tomography, it is possible to quickly, cheaply and reliably evaluate the state of the hip and positions of femoral bones before and especially - after the treatment. This naturally increases the risk of cancer associated with elevated levels of ionizing radiation, which pediatric patients are more sensitive to.

In order to find the lowest dose that can be achieved, while still maintaining acceptable image quality for anatomical evaluations, a phantom based noise simulation technique was used. This method was chosen for its retrospective approach - during the simulation procedure, old images, obtained from various patient scans is used and a certain amount of noise, corresponding to specific CT scanning parameters, is added to them. Using this method, it is possible to estimate the impact of these parameters on the image quality, more specifically – noise, since the main challenge of using low dose CT scans is high level of noise present in the image.

The aim of this work: Optimization of the pediatric developmental dysplasia of the hip computed tomography protocol, using the results from the evaluation of images with simulated noise.

Tasks for the thesis:

- To identify noise affecting scanning parameters and create a phantom corresponding to the developmental dysplasia of the hip case.
- To generate the reference noise samples for the DDH case.

- To construct and apply the phantom based noise simulation algorithm for images of developmental dysplasia of the hip.
- To evaluate the impact of noise on the image quality and clinical acceptability, in the simulated images.

1. LITERATURE REVIEW

1.1 Developmental dysplasia of the hip

1.1.1 Causes, epidemiology

The hip joint is an important part of the musculoskeletal system. It enables a wide array of movements from walking to running and jumping. The hip joint is classified as a multiaxial, specifically – a ball and socket synovial joint and it is formed between the hip bone that has a round, cup shaped structure called acetabulum and the head of the femur. The developmental dysplasia of the hip (DDH) is a disorder where the hip joint is not formed normally during infancy and the head of the femur is loose in the hip socket.

The dysplasia or dislocation of the hip can manifest on both hips or only on one side. DDH of both hips is less common and makes up ~40% of all cases. The prevalence of clinical hip instability ranges from 1.6 – 28.5 cases per 1000. DDH most commonly manifests during the birth or the first 2 – 8 weeks (60-80%), however it can also develop during the first 6 months – 2 years. Screening of newborns for DDH is a common practice and it is used to detect the pathology early and correct it. However, some cases are more severe or can be misdiagnosed entirely, in which case a more serious treatment is required (1).

Risk factors:

- Gender –male: female ratio is ~1:8.
- Unusual fetus position, lack of space in the womb.
- Fetus hypertrophy.
- First born, twins.
- Family history.

There are four main stages of pathological hip development:

A. Normal hip joint.
B. Dysplasia coxae – the dysplasia of the hip when the joint is not fully developed, but the head of the femur is still in the acetabulum.
C. Subluxatio coxae congenita – subluxation, when the head of the femur is partially displased from the acetabulum.
D. Luxatio coxae congenita – dislocation, when the whole head of the femur is removed from the acetabulum.

1.1.2 Imaging methods

For clinical diagnosis of DDH some form of imaging is necessary for precise evaluation of the hip joints. Palpation and various functional tests are used during routine inspections by the physician for the initial diagnosis. Advanced imaging methods used are (2):

- Ultrasonographic assessment.
- Radiographic or computed tomography assessment.
- Magnetic resonance imaging.

Ultrasound is used for patients up to 6 months of age. Using a 5MHz or 7.5MHz transducer, it is possible to evaluate cartilage tissue of the hip joint that is not yet ossified. This method is also useful in that the evaluation can be achieved in real time and an additional assessment of the stability and mobility of the joint is possible. Two angles are derived from the sonogram (1):

- α angle – evaluation of the roof of acetabulum.
- β angle – evaluation of the femoral head.

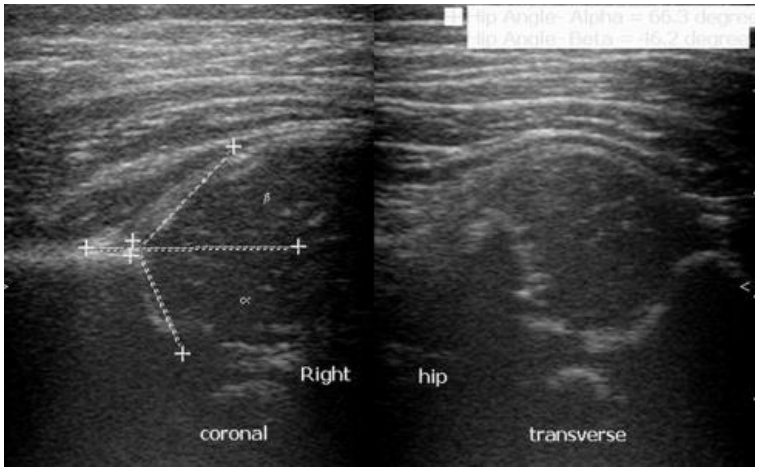

Fig. 1. Sonogram of the hip joint (3)

Usually, a radiographic evaluation is reserved for older patients – from around 4 – 6 months, since up to 4 months it is not informative enough to be justified. However, after the bones are ossified, and ultrasound examination provides less information, symmetrical plain film assessment of the hips is used to determine the relationships between the structures of hip and femur. Using this method, the physician is evaluating the Hilgenreiner, Perkin and Shenton lines as well as acetabular index (2).

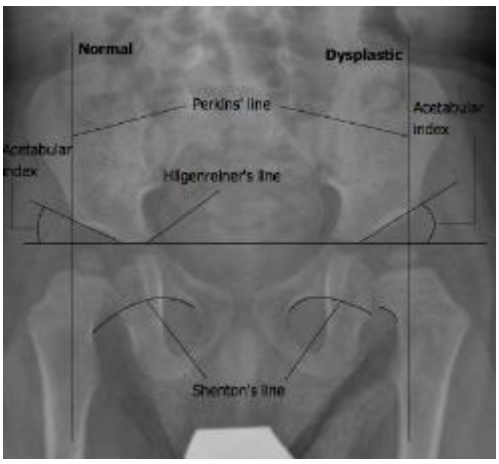

Fig. 2. Evaluation lines for DDH (1)

Although plain film assessment can be considered a useful method for diagnosing DDH, the postoperative control is another subject. Due to the plaster casting after the reduction called hip-spica cast it can sometimes be difficult to produce acceptable radiographic images for postoperative and follow-up control of the procedure. This can sometimes lead to the repeated exposures. Furthermore, 2D projections of the femoral head and the hip usually do not provide enough information for a complete evaluation and postoperative control. Due to this, imaging methods with 3D reconstruction capabilities are more suited for these situations as described in (2,4,5).

Computed tomography and magnetic resonance imaging (MRI) are both useful modalities for assessing the quality of reduction after the procedure. MRI, however, is not routinely used. MRI can be used to control the femoral bones and hip placement, since it does not use ionizing radiation during examination and because good images of the soft tissues may be obtained. The main disadvantages of magnetic resonance are time, cost and the need for additional anesthesia during the procedure. Computed tomography on the other hand can be used immediately after the reduction to confirm its success, since there is usually no need for additional sedation. The scan, therefore, is done much faster and the examination is cheaper, as compared to MRI. Also, using 3D reconstruction it is possible to further evaluate the positions of the femoral bones relative to the acetabulum (2,4).

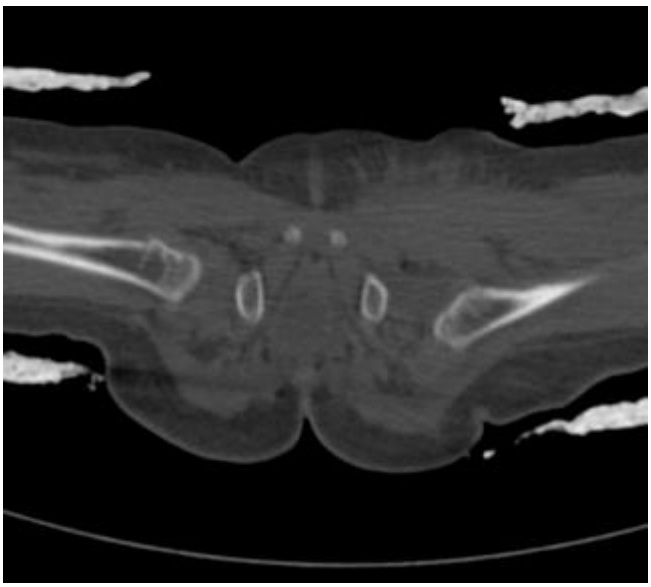

Fig. 3. Image of a CT scan slice

Most common CT scanning type for DDH is axial scan, using 0.5 – 1mm slice thickness. Recommended protocols usually use 100 – 120 kVp, automatic exposure control, with the reference mAs of 110. Reconstruction algorithms can also vary, but usually involves a soft tissue and bone filter reconstructions. The bone filter reconstruction allows for better viewing of the femoral bones and the hip, providing better control of the postoperative hip-femoral angle evaluation. The soft tissue reconstruction is used for 3D evaluation of the femoral bone positioning in relation to the acetabulum. Although image quality of the scans made using CT is very good, for evaluation of the post reduction and further control of the pathology, is not necessarily required. Even in images with a significant amount of noise it is possible to clearly see the main anatomical structures that need to be evaluated (4,5).

1.2 Noise simulation approaches

Simulating low dose scans is a useful technique, when optimization of CT protocols is required. Using various different approaches, it is possible to estimate the lowest dose for different diagnostic evaluations, where there is still enough information to provide a reliable diagnosis. Simulated scans can be used for optimization of new or currently used reconstruction algorithms that can reduce the noise in images of similar low dose scans.

There are many different noise simulation tools and techniques used today and over the years (6-14), overall they can be separated into two main branches:

- Adding noise on the image in existing image space.
- Adding various types of noise on the raw projection data.

Talking about the latter, there are multiple approaches for this method and currently, some of the main computed tomography scanner manufacturers provide additional software or noise

simulation tools devoted specifically for research purposes. For example, there are noise simulation tools available from GE Medical Systems (6). This tool uses the existing raw data from the scan to produce noise at predefined tube parameters, usually lower current (mA). Then, by reconstructing these data sets, images with representative noise levels can be viewed. This and other similar simulation methods use a simple noise addition model, where it is assumed that it is possible to add Gaussian noise to the scan sample from the original scan with higher dose and mAs (7).

Since it is known, that quantum noise is proportional to the inverse square root of the photon count in the detectors and the data sample of a CT scan is the amount of photons detected multiplied by the gain coefficient, it is possible to derive the additional noise related to the lower scanning parameters:

$$\sigma_a = \beta\sqrt{P(\frac{1}{\alpha} - 1)} * R_n; \quad (1)$$

here, σ_a is the noise to be added to the raw data. β is the scaling coefficient, that is dependent on the system of data acquisition. a is the current reduction coefficient. P is the signal level for the data sample. R_n is the normal noise generator output.

The overall noise is not just simply photon quantum noise, by analyzing low signal levels there is additional electronical noise that is present from the acquisition system itself. This can also be added to the final simulation, by creating another coefficient to add more Poisson noise to the final image.

$$\sigma_a = \sqrt{P(\frac{1}{\alpha} - 1)} * R_n * N_n; \quad (2)$$

Here, N_n is an additional normalization coefficient $N_n = \beta * N_q$ that is used to account for the additional noise sources. There are multiple different approaches of this kind in literature and each have various takes on the noise distribution evaluation and modification, however the main principle remains the same.

In one article from 2010, a low dose simulator, made using this approach, showed a good similarity between the actual low dose scans and simulated low dose scans (9). In another article, also from 2010, using another simulator made using the raw data simulation technique, reached the conclusion that it is possible to simulate valid images by reducing the mA up to a 100 times. The main point here, is that by having a good reference point – images made with high mAs, there should be no problem in simulating images at very low – 20 or 12 mAs (10).

Such noise simulation tools and techniques are indeed useful and provide reliable noise representations on the simulated images. However, application of this method is only possible, when researchers have access to the raw transmission profile data from the scans. This can be difficult to acquire not only because some CT scanner manufacturers outright deny access to such information, but also due to the fact that some scanners do not allow the export of raw data files and only the last 30-60 scans are stored in the memory of the scanner. This can be a problem, when dealing with rare clinical cases, since only a few of them might be scanned every year. As such, collecting a sample of raw data files of a significant size for simulations and research purposes can be a challenge in the beginning and could take years to acquire. However, with regular image files, they can be stored and exported without any problem. Although they do not contain as much information, it is still possible to use them for retrospective noise simulation and evaluation.

When there is no possibility to access or acquire raw CT scan data, there are two main options for simulating noise using the available conventional CT image data. These are the virtual synthetic noise sinogram generation method and phantom based noise simulation approaches. Both of these methods are similar, as the end simulation product is a generated synthetic noise image that is added on to the original CT image to produce the final simulated image obtained with lower dose and higher noise level. The generation of this synthetic noise image is where these methods differ.

The virtual sinogram generation method algorithm starts by converting the original CT image matrix with HU (or CT number) basis into one with the attenuation coefficient basis. A virtual sinogram needs to produced using a virtual projection, that uses line integrations of the attenuation coefficients along each X-ray beam path between the detector and the beam source. Produced virtual sinogram represents each gantry step and detector location related linear attenuation coefficient (11). From here, the virtual sinogram data translation to virtual linear sinogram is performed:

$$S_v(g,d) = Q_0 * e^{-A_v(g,d)}; \quad (3)$$

Here, $A_v(g,d)$ is the virtual sinogram. g is the gantry step in CT and d is the location in the detector array. Q_0 is the incident photon flux during the CT scan.

Then the required amount of simulated synthetic noise can be calculated by the equation:

$$\sigma^2{}_{simulated}(g,d) = \alpha * Q_0 * T_v(g,d) * \left(\frac{1}{\rho} - 1\right) + N_s; \quad (4)$$

here α is the correction coefficient derived from NPS curve analysis of the original and simulated image. ρ is the ration of simulated mAs and the original mAs. N_s is the system noise factor.

Finally, the synthetic noise can be generated by multiplying the SD by white Gaussian noise, pixel by pixel, and added to the virtual linear sinogram:

$$S_{simulated}(g,d) = S_v(g,d) + \sigma_{simulated}(g,d) * WGN; \quad (5)$$

The combined virtual linear sinogram is then reversed back and a virtual noise sinogram is produced that can be subtracted from the original one, producing final simulated noise sinogram. Then, all it takes is to reconstruct it into CT image with HU based matrix and adding it to the original image matrix (11,12).

These kinds of approaches to noise simulation are interesting, in that they essentially operate using sinograms, which is useful when reconstructing the image back into HU based form. However, the initial evaluation of the original CT images that is required, is based on the measurements of NPS and MTF curves, which can differ depending on the image compositions. Furthermore, there is a need to evaluate parametric CT scanner values – the actual initial photon flux on the detector array during the examination and the system noise of the scanner. This can usually be done only by using outside knowledge from literature and can be a cause for inaccuracies. Also, half of the reviewed virtual sinogram generation algorithms use some part of raw data from the CT scanner.

Phantom based simulations, meanwhile, operate in image space, on the basis of additivity of variance between two independent scans (15-17). If the difference in the attenuation between them is divided by a √2, an unbiased sample of the noise can be obtained. This is why it is possible to add such a generated noise sample from a scanned phantom on to the CT image scanned with a higher mAs parameter and possessing a higher amount of noise. By combining the original image pixel variance, which will be lower, with the noise sample, it adds up and increases the variance of the original image. The end result is an image – a pixel matrix, whose variance (noise) is increased by a set amount, representing the lower mAs scan. This method does not require raw scan data, or complex calculations, however it has to be specifically adapted for each case.

To summarize, in all of the studies found in literature, that were using these various noise simulation approaches (6-17), authors agree, that the images obtained with these methods are a good representation of low dose CT scans and can be used when optimizing various CT protocols, or when testing the various new reconstruction algorithms. On average, in these

studies, the difference in noise, in the simulated images, was always less than 5% from the actual, low dose scan images, be it phantom scans or actual patient scans. Although the best results – the most accurate noise simulations, come from the methods that use raw scanning data, when such information is unavailable, virtual sinogram generation or phantom based simulations are just as effective.

1.3 Dose and optimization

In computed tomography, one of the main parameters, describing the radiation that the patient is exposed to, is called the computed tomography dose index (CTDI). This value describes the standardized CT radiation output, to a standard size phantom during an axial scan, therefore it shows how much of it is deposited in a single slice. This is based on the fact that tissues, that are in a single slice, get irradiated not only when the beam passes through it, but adjacent slices as well. CTDI describes the average dose along the z-axis of the scan (18):

$$\mathrm{CTDI} = \frac{1}{\mathrm{NT}} \int_{-\infty}^{\infty} \mathrm{D(z)dz}; \quad (6)$$

here, D(z) – radiation dose profile along the z-axis of the scan; N – slice number used during the axial scan; T – slice thickness.

In practice, there are a few different types of CTDI used.

- $\mathrm{CTDI_{100}}$ – it is measured using an 100mm ionization chamber. Scanning is done using standardized phantoms – 16 cm Ø head phantom and 32 cm Ø body phantom (18,19).

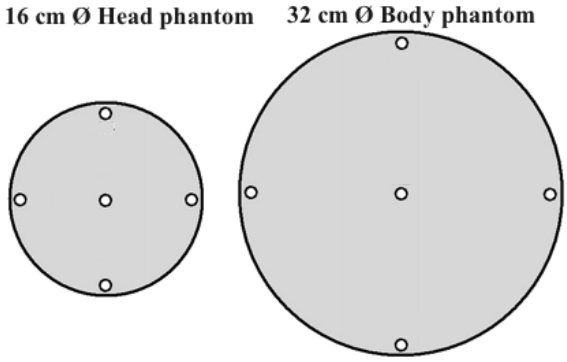

Fig. 4. Head and body phantoms (18)

- $\mathrm{CTDI_w}$ – since CTDI described dose can differ inside the center of the phantom and the periphery, in order to evaluate it more consistently a weighted CTDI is used.

$$\mathrm{CTDI_w} = 1/3\ \mathrm{CTDI}_{100,\mathrm{center}} + 2/3\ \mathrm{CTDI}_{100,\mathrm{perif}}; \quad (7)$$

- $CTDI_{vol}$ – in helical scanning, a new parameter is introduced, called pitch – the travel of the table per rotation, divided by slice thickness. So, depending on the pitch, if it is >1, the $CTDI_{vol}$ spreads the dose of $CTDI_w$ over a longer z-axis length of the scan and vice versa if it is <1. We can then describe CTDI it as:

$$CTDI_{vol} = 1/\text{'pitch'} \times CTDI_w; \quad (8)$$

However, CTDI is only an approximation of the average dose in the irradiated volume. In order to evaluate the total amount of dose the patient receives, another metric is used and displayed in most modern CT scanners, called dose-length product (DLP). It better represents the overall absorbed dose, delivered over the full length of the scan (19,20).

$$DLP\ (mGy\text{-}cm) = CTDI_{vol}\ (mGy) \times d\ (cm); \quad (9)$$

The three cornerstones of radiation protection in medical applications are justification, optimization and limitation. Since the theme of this thesis is optimization, it states that every examination must be made in accordance to the ALARA principle – as low as reasonably achievable.

In pediatric diagnostics, CT is a useful imaging modality, however, due to its high ionizing radiation output, it is used sparingly (21). Over the past 10 years a lot has been done in the field of dose optimization for children. One of the leading coalitions of health care organizations - The Image Gently Alliance, active since 2007, has been actively pushing for practice changes in pediatric imaging. Due to rapid evolution, change, and availability of CT technology, the protocols and practices should be changed as well (22).

Since in pediatric CT diagnostics the patients are much smaller than the adults, and knowing that the CTDI values, from the scan data, are only referencing the CT scaner outputs for standard 32 and 16 cm phantoms, there is a clear problem when estimating the actual effective doses received by the patient. If the standard 32 cm body phantom is used as a reference, this could lead to a dose difference of up to 2-3 times. In regard to this, American association of physicists in medicine (AAPM) has released a report in 2011, describing size-specific dose estimate values (SSDE). SSDE tables allow for better evaluation of the actual dose to the pediatric patient, using the $CTDI_{vol}$ value from the scan (23).

Effective doses in CT are usually described using the dose length product (DLP). Using both CTDI and DLP values it is easy to compare different CT protocols and the doses received from them. Using SSDE coefficients and combining them with DLP or CTDI values of a scan, according to various articles, the actual CTDI for abdominal scans would have to be 50% higher and twice as high for the cardiac CT scans. Comparing CTDI from a 10 cm phantom and the

standard body phantom, according to one research, the doses would be higher up 2.6 times (20). In another article, calculating the dose using the new ICRP 103 conversion coefficients, the actual doses to the pediatric patient head scans were 11 % higher, 20 % higher for chest scans. These conversion coefficients were used to modify the DLP values of CT scans (24).

Since image quality in CT imaging is the main concern, with noise and contrast being its properties, the primary parameter that is being changed, when optimising CT protocols, is the tube current (mA) or exposure - current-time product (mAs). Exposure is also directly proportional to the dose received by the patient during the scan, this is another factor why mAs is usually the main parameter changed when optimising various CT protocols (25). There are two main practices for it:

- Fixed tube current protocols.
- Protocols that use tube current modulation.

Fixed tube current protocols usually use some sort of indication based system, based on either research or common practice knowledge. Depending on the specific indication or diagnosis of the patient or specific anatomical area, the operator selects the scanning protocol and changes parameters manually if needed. This is usually done when there is a need to adapt, depending on the patient size, age or indication (26). Obviously, this requires that the operator has sufficient knowledge about the CT scanning parameter influence on image quality. When comparing the same anatomical area of pediatric patients and adults, a significant difference in the scanning parameter values. For example, body scan for pediatric patients can only require 4-6 times lower mAs values than for adults, to achieve images of the same quality (27). This in effect reduces the dose to the patient by the same factor. So, all in all, manual tube current manipulation/reduction is the most straightforward way for optimizing CT protocols, however it requires a lot of experience from the operator, in order for it to be safely implemented.

Tube current modulation is the method based on different attenuation in the human body along its z-axis and transverse directions (angular modulations). During z-axis modulation the scanner takes into account the different attenuation of the patient in different anatomic areas along the scan length. These attenuation values are usually taken during the initial "scout" before the scan. The angular modulation means that the current is modulated between lateral and AP positions, using attenuation values from the scout or a previous 180º or 360º projection. Combined, these two methods can decrease the entrance doses up to 70% (28). All that is needed from the operator is to choose the image quality, be it the noise index or other parameter that can differ depending on the manufacturer.

Automatic exposure control (AEC) is the modulation of the tube current in real time, using the beam intensity data from the detector matrix. Each manufacturer has their own algorithms for

AEC systems and knowing them is important when optimizing CT protocols. Siemens uses quality reference mAs system, that describes the effective mAs (mAs/pitch) for required image quality, scanning a standard or pediatric size patient. Philips uses a reference image, from previous reference case, that provided acceptable results and is used for comparison in future scans. GE uses noise index, which is the standard deviation of pixel values in a specifically sized phantom, compares it to the patient scout and accordingly adjusts the modulation to achieve the same image quality (29). A few studies comparing the AEC of different manufacturers have been conducted, however no significant differences between them were found.

AEC is the main tool of optimization in modern pediatric protocols. Since most of the manufacturers provide preinstalled protocols in their CT scanners, using a pediatric protocol is generally simple – choosing the recommended (default) noise index or other manufacturer equivalent image quality measure and checking the AEC box. Then all that remains is to properly prepare and center the patient for scanning, which is also a very important part of the procedure, since improper centering can also lead to increased dose to the patient (30). This in principle works well and most of the time pediatric patients get the lowest dose possible. However, there are certain indications, where good image quality may not be necessary in order to make the correct evaluation of the pathology. In these cases, it is possible to lower the dose even more, either by using manual settings or with lower AEC image quality metrics. Therefore, this work will discuss the possibility and viability of lowering the scanning parameters in one such case, when scanning for evaluation and control of DDH.

Another approach to the optimization of CT dose is using various new reconstruction algorithms. With modern CT scanners there is a possibility to use new types of iterative reconstructions. These algorithms work by making use of using noise statistics and making more complex assumptions during the reconstruction process, in order to combine this information with multiple iterations of the reconstruction. This process is called statistical iterative reconstruction (SIR) and is more complicated, therefore it takes more time and computational resources to fully reconstruct the image. On the other hand, these types of reconstruction algorithms provide a significant decrease in image noise, therefore it is possible to achieve the same image quality using much lower scanning parameters, and effectively – doses (31). There are also many different versions of these algorithms, such as adaptive SIR, which begins the reconstruction after an initial standard filtered backprojection. This type of reconstruction can decrease the dose (by improving the image quality) by up to 40% (31).

The best results are achieved using so called full model iterative reconstructions. They operate using the raw data of the scan, without the initial filtered backprojection. By using both backprojections and forwardprojections based on statistical models and modeling the x-ray

beams using all the scanning data, obtained from the raw scan data and comparing them, the algorithm can determine the difference between them. By doing this a number of times, until the difference becomes very small, it produces images that have outstanding quality at low doses. A study researching this algorithm found that using this algorithm it is possible to reduce the noise (or the dose) up to 90%, comparing to the basic CT reconstruction (32). However, the downside is that the process is very time consuming and computationally demanding.

2. THEORY

2.1 Computed tomography

2.2.1 Working principle

Computed tomography (CT) is an imaging modality, widely used in a large number of diagnostic fields since its introduction in 1971. Its speed and precision, as well as its ability to produce high quality images, are the main reasons why it is used in almost every hospital in the world. The images in CT are acquired using the measurements of the X-ray transmission profiles of a patient from a number of angles. By rotating the X-ray tube and the large row of detectors around a patient, transmission profiles from each scan are acquired and are used for image reconstruction.

The image consists of a matrix of pixels, each with its own value, corresponding to the linear attenuation coefficient μ of the corresponding tissues. An attenuation coefficient depends on the material composition, electron density and the energy of the beam photons (33,34).

$$I(x) = I_0 e^{-\mu x}; \tag{10}$$

here, x is the thickness of the material, I(x) is the attenuated X-ray beam's intensity and I_0 is the initial beam. As the X-ray beam travels over the length of the patient's body, it is attenuated by different tissues, having different compositions and densities, therefore having various different attenuation coefficients. If the beam travels through the patient over distance x, over regions with different linear attenuation coefficients μ_1 and μ_2 then its transmission profile would be:

$$I(x)=I_0 e^{-(\mu 1 x 1+\mu 2 x 2)}; \tag{11}$$

Therefore, the transmission over 'n' regions having various linear attenuation coefficients will be:

$$I(x) = I_0 e^{-\sum_{i=1}^{n} \mu_1 x_1}; \tag{12}$$

Although it is impossible to determine every single separate attenuation coefficient from one transmission measurement, using a huge number of such measurements at different angles over the same imaging plane, it is possible to calculate and separate the coefficients. Distributing them over the plane of the measurement and assigning them different gray-level values in an image matrix, the image corresponding to the patient cross-section can be obtained.

2.2.2 Basis of the image matrix

Such image matrix, comprised of pixels with different linear attenuation coefficients of the material, is then transformed to a Hounsfield unit (or CT number) matrix (31). Here:

$$\mathrm{HU_{mat}} = \frac{\mu_{mat}-\mu_{water}}{\mu_{water}} * 1000; \quad (13)$$

here, $\mathrm{HU_{mat}}$ represents the assigned pixel CT number, μ_{mat} represents the attenuation coefficient of the material, μ_{water} is the known linear attenuation coefficient of room temperature water. Therefore, this distributes the typical tissues in the human body over a scale that's relative to water.

Table 2. HU scale

Tissue	Air	Lung	Fat	Water	Blood	Soft tissues	Bone
HU value	-1000	-750	[-100,-80]	0	[+50,+60]	[+100,+300]	[+300,+2500]

Creating a Hounsfield scale ranging from -1024 to +3071 HU uses a minimum of 12 bits. Visualization of a CT image is usually done using an 8bit grayscale with 256 gray-values. Each pixel is then mapped to an 8bit "window" value. The central value of the HU map is called the level of the window. By changing the window width – the range of the HUs represented in the image matrix it is possible to clearly visualize a variety of different tissues in the image.

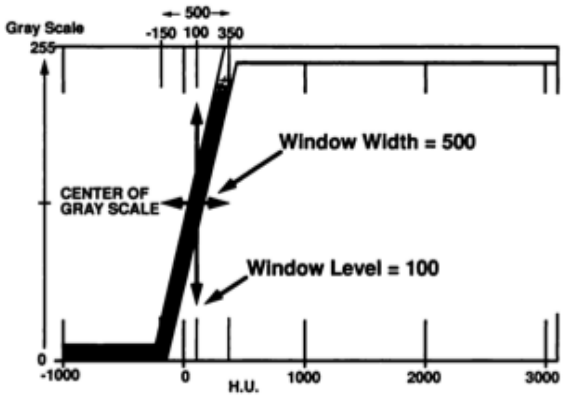

Fig. 5. Window level and width representation (32)

2.2.3 Reconstruction

In order to reconstruct the image from detected beam intensity, various algorithms are used to produce an image with acceptable visual quality. Modern CT scanners generally tend to use backprojection based algorithms, mainly – filtered backprojection.

In backprojection, every X-ray beam path, that is crossing the patient's body, is divided into equally spaced elements. Then, it is assumed that each element is equally contributing to the total summed linear attenuation of the beam. As mentioned before, there is a need for multiple angle transmissions, in order to have a sufficient amount of information to identify a final complete attenuation coefficient for a single element. After the backprojection is complete for every element, a matrix of pixels representing final attenuation coefficients are assigned their HU values and then the image is complete and can be viewed (35,33).

Backprojection axis of projection can be described as:

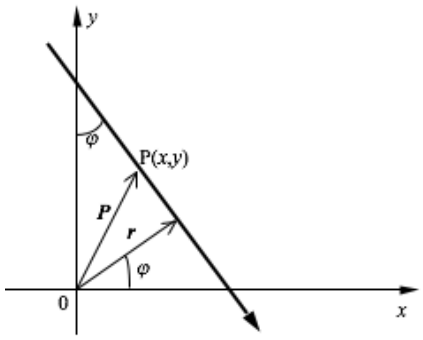

Fig. 6. Axis of projection (33)

If a beam is crossing the 'x' axis, its orientation is described by the angle 'φ' and its distance 'r' from the 0 coordinate. If we take any point on this plane – 'P(x,y)', it can be described as a vector P = I x + j y. Then, a projection of 'P' into 'r' is their scalar multiplication – r = P • r, or x cos φ + y cos φ. Using this relationship, the point P(x,y) is bound to the beam that crosses it with coordinates (r, φ).

By using these relationships, all that is left is to calculate for the image pixel's total linear attenuation coefficient μ = f(x,y). This requires calculation and storage of every summed linear attenuation coefficient into the memory of the computer. These attenuation coefficients are marked using the X-ray beam coordinate parameters–- 'r' and 'φ'. If any two beams cross the point of interest P(x,y), then their summed linear attenuation coefficients will be identified and stored in the memory as $p_{xy}(r_1, \varphi_1)$ and $p_{xy}(r_2, \varphi_2)$. All in all, for every point of (x,y) computer selects all the summed attenuation coefficient values from all the beams that crossed it and adds

them together (35). By the end, the final image pixel value (total linear attenuation coefficient) can be described as:

$$f(x,y) = \sum_{i=0}^{N-1} p_{xy}(r_i, \varphi_i); \quad (14)$$

here, N – the number of projections.

Although a simple backprojection is capable of producing an accurate image, its overall quality is poor. Images from unfiltered backprojections are muddled and blurry and therefore not useful, when in depth evaluation of anatomical structures is necessary. To eliminate this problem, filtered backprojection method is used in most modern CT scanners. By using convolution of 1-D integral equations to reconstruct 2-D images, an additional filter function is added on the raw transmission profile data before the backprojection.

These deblurring functions, also called convolution filters or kernels, work by removing different frequency components in the Fourier's frequency domain, where they are removed or softened, in order to provide a more useful image. It uses a one dimensional filter kernel on every transmission profile. When it is transformed back from frequency space using inverse Fourier transform, the image is much clearer and less blurry. These convolution filters can vary and provide different information using the same transmission data. For example, using low frequency (or a high-pass) filter, that essentially reduces all low frequency signals and ignores high frequency signals, can enhance the edges of objects in the image and increase the overall sharpness and vice versa – a high frequency kernel can smooth the image and decrease the amount of noise present (35,36).

Most of the time, a filter, that blurs the image a bit, is chosen. The reason being, that a blurry filter can decrease the overall amount of noise in the image. Images that are too sharp suffer from a lot of noise and therefore makes it difficult to make diagnostic evaluations in most cases. In case there is a need for a sharper image, all that is needed is to make a reconstruction with a different filter kernel, which is a simple operation on most modern CT scanners (33).

All of the algorithms that are using filtered back projection (FBP) are part of the analytical reconstruction family. Each CT scanner manufacturer has their own different take on such reconstructions. For example: GE medical systems use 3D weighted FBP, Philips use COBRA nPI, Siemens use AMPR and 3D weighted FBP. All of these analytical recon's have a good balance between accuracy, computational and dose efficiency. As mentioned before, every manufacturer also has their own statistical iterative reconstruction algorithms.

2.2 Image quality

Computed tomography image quality depends on 4 main image parameters (18,38).

- Contrast.
- Spatial resolution.
- Noise.
- Artifacts.

Together, these four parameters determine the visibility of anatomical structures and suitability for an accurate diagnostic evaluation.

2.2.1 Contrast

Image contrast depends on the object and display contrast. Display contrast depends on the selected window level and window width, which can be different and easily changed. The object contrast depends on its attenuation, since different types of tissue have different electron densities and therefore–- attenuation properties. Image contrast can be defined as the difference in the gray-scale values, between two adjacent regions. CT, as an imaging modality, is considered to have a high sensitivity to contrast, due to the possibility to display different structures by manipulating window settings (33,18,37).

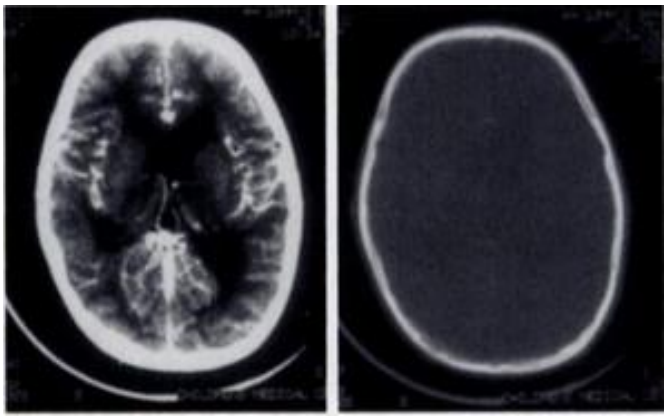

Fig. 7. Window level of 50 on the left and 2500 on the right (33)

Figure 8 shows, that by using a smaller window level it is possible to better visualize soft tissues and when the window level is wide – only bone structures can be seen.

2.2.2 Spatial resolution

Spatial resolution is defined as the ability to differentiate between small objects in close proximity to each other. This is usually determined using special line-pair testing patterns, usually inside phantoms.

The spatial resolution of CT can depend on a few factors. From physical – the detector element size and amount, from focal spot of the x-ray generator and the focal spot-object distance. It can also depend on the slice thickness – spatial resolution is higher with thinner slices and vice versa. It can also depend on the reconstruction filter kernel used during filtered backprojection. If the selected filter is high-pass or sharp (bone) filter, the spatial resolution increases – it is possible to differentiate more line-pairs or see more detailed anatomical image.

2.2.3 Image Noise

In computed tomography, like in every x-ray imaging modality, noise present in the image is of a statistical nature. Generally, noise depends on the amount of x-ray photons that reach the detector matrix (quantum noise). It also depends on the detection systems intrinsic electronic noise and the reconstruction used. Usually the latter two are less predominant in the image, so the main noise influencing image quality is considered to be quantum noise.

As mentioned before, noise is of a statistical nature. Noise itself is the variance of the beam intensity, that is caused by the generation of x-rays. Generated x-ray photons fall under Poisson distribution and so, the quantum noise is proportional to $\sqrt{N}$, when N is the number of photons. When reconstructing the image, the noise in it, would then be proportional to $1/\sqrt{N}$. To put it simply, since N is the amount of photons used when producing an image, it is directly related to the tube current parameter of the CT scanning system. In previously described noise relationship, N is the number of photons, therefore by changing the mAs of the CT scan, noise in the image approximately changes proportionally to $1/\sqrt{mAs}$ (38).

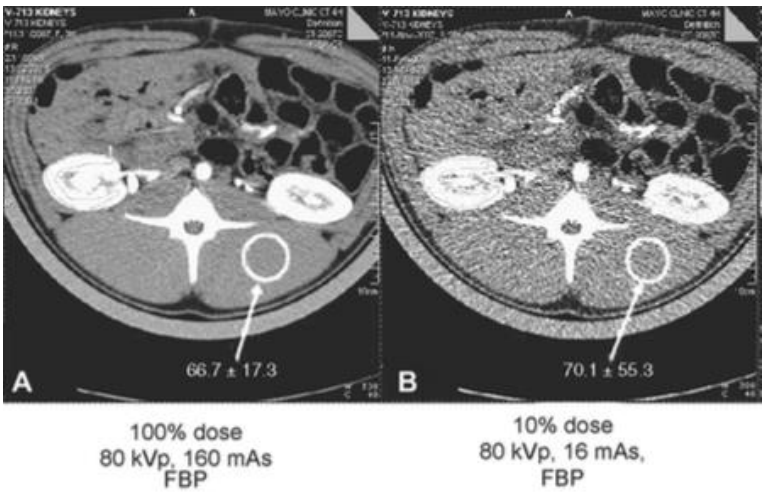

Fig. 8. mAs influence on image noise

Overall, there are 5 main parameters of a CT scan that can influence image noise:

- Tube potential, peak kilovoltage (kVp).
- Tube current, amperage (mA).
- Scan time (s).

- Slice thickness/detector matrix size.
- Reconstruction filter (although not directly linked to the x-ray photon count).
- Scanned object size.

Noise in CT is the random variation of CT numbers (or HU) from a central mean value. In order to measure and evaluate noise, selection of a specific region or area, in which this variation can be measured, is required. These regions of interest (ROI) can be rectangular or oval and are used when scanning uniform phantoms, in order to evaluate the standard deviation and average pixel values inside. Standard deviation (SD) is usually the main measurement of noise. After the scan, most CT workstations allow for these measurements and user can choose their ROI on the different parts of the image to see what the SD is inside (38,39).

2.2.4 Artifacts

Artifacts in computed tomography are the inconsistencies between the real tissue attenuation and reconstructed HU values in the image, since the reconstruction algorithms operate under the assumption that every measurement is correct and consistent. The errors and inconsistencies are especially visible in CT scans, where the image is reconstructed from a huge number of measurements. Artifacts can be various and can be sorted by different categories – physics based, patient based, scanner based, reconstruction based, all of which can be present in the image. They can also be sorted by their type – shading artifacts, ring artifacts, streaking artifacts (18,40).

Most common type of artifact, and the one most relevant to this thesis, is a shading type artifact called beam-hardening artifact. It is presented in practically every CT image. Although modern CT scanner reconstruction algorithms are made to mitigate and correct most of such artifacts, sometimes they are still clearly visible. Beam hardening artifacts are of physical origin: when the x-ray beam passes through the body, some of the low energy photons are absorbed. From this interaction two types of artifacts can be present in the image – cupping artifacts and streak artifacts (18,39).

Cupping artifacts are caused when photons are passing through the middle (center) of a uniform spherical phantom. Since photons traveling through the periphery are hardened less, than those traveling through the center, as the beam hardens, its attenuation rate decreases and therefore the beam becomes more intense than expected, when reaching the detector matrix. In the end, the transmission profile becomes different than the ideal profile that would have been obtained without hardening and the resulting CT numbers in the image form a specific cupped shape (39).

Meanwhile, streak artifacts appear in cross sectional areas that are heterogeneous, usually between two dense objects. Its source is the inconsistent beam hardening, since at different tube positions the beam passes through only one of the objects and on others – through both of them. Such inconsistencies cause dark streaks after the reconstruction. It is important to note, that such streaks are also caused by photon starvation, which takes place, when the beam travels an unusually long distance and over highly attenuating regions throughout the body, usually through the shoulders or in the case of this thesis – widely spread legs (hip and femur). If the tube current is low, in these horizontal projections a relatively low number of photons reach the detector matrix. This causes noisy projections and after the reconstruction the noise is amplified even more, showing up as dark streaks in the image (18).

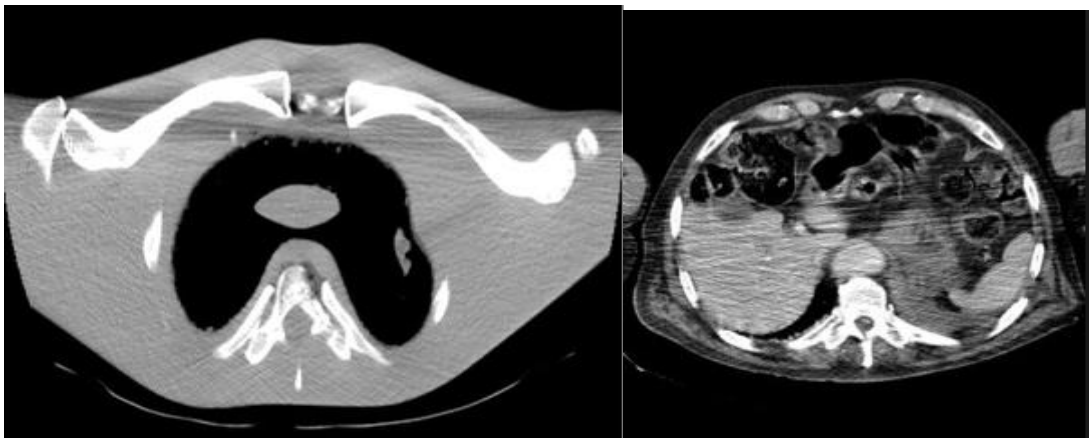

Fig. 9. Streak–- photon starvation artifacts (39)

3. MATERIALS AND METHODS

3.1 Subjects and scanning protocol

The study was conducted in Vilnius University Hospital Santaros Klinikos Children's Hospital. For this study, computed tomography scan data from 31 patients was obtained and after analysis and comparison of various scanning parameters 20 were selected for the simulation process. The patient scans were selected using these criteria:

- Same tube voltage – 120 kV.
- Slice thickness – 0.75mm.
- Reconstruction kernels B20.

Other scan parameters – such as exposure (mAs), reconstruction field of view (FOV), patient size, age, gender were various.

Table 2. Patient characteristics

	Age (months)	mAs	rFOV	DLP	$CTDI_{vol}$
Mean	11,1	86,56	260,6	94,3	6,8
Standard Deviation	11,5	50.8	62,7	55,3	3,9
Min	1,7	36	161,0	40,8	2,8
Max	42,3	221,1	416,0	247,0	15,1

All patients were scanned using the same "Siemens Somatom Sensation 64" CT scanner. From these patient sets, 20 sets of images were reconstructed using B20 kernel.

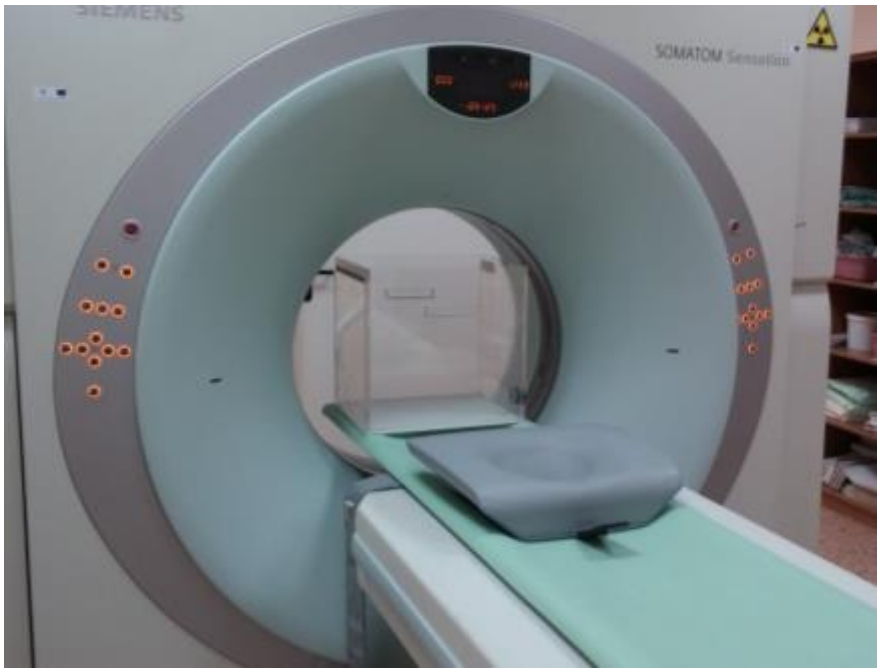

Fig. 10. "Siemens Somatom Sensation 64" CT scanner

Since the modern approach to the optimization of the dose to pediatric patients is based on application of the automatic exposure control during the scan, every image was made using different exposures. Since this is done automatically and the exposure cannot be modified once AEC is selected (other than selecting the maximum reference mAs and noise index), by using manual settings it would be possible to significantly reduce the tube current and therefore the dose.

3.2 Phantoms

A gelatin based phantom was made and scanned at various tube exposure parameters in order to obtain the noise samples for the simulations. Phantom size was selected to be approximately the width and thickness of the largest patient. Phantom dimensions – 400x200x300mm. Water to gelatin ratio was 100ml:5g, total of 30l. Gelatin type phantom was selected due to safety concerns regarding the volume of the water that would otherwise have to reside over the CT scanner gantry and to eliminate movement of water during scanning process. Measured phantom HU - ~10 HU, which is just slightly above water at 0 HU (table 1.).

The scans were made at exposures of 13, 20, 50 mAs. These exposure parameters were selected after reviewing scan data of the selected patients.

Another spherical phantom of ø270mm was scanned and using the scan data the size-noise dependence curves at various tube exposure parameters were obtained. Both phantoms were scanned using the same "Siemens Somatom Sensation 64" CT scanner as the original patients.

Fig. 11. Phantoms used, gelatin based on the left and spherical on the right

The spherical phantom was also wrapped in a plaster cast, using the same technique that is used when immobilizing children after the reduction of developmental dysplasia of the hip, in order to evaluate its impact on the image noise.

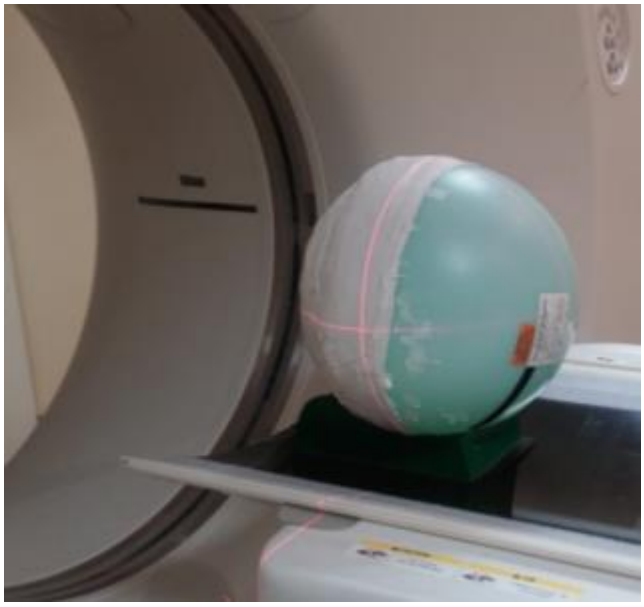

Fig. 12. Phantom with plaster casting

Scan protocol:

- Axial scan mode.
- Slice thickness – 0.75mm.
- 120 kV.
- AEC off, effective 13, 20, 50 mAs.
- Pitch – 1, rotation time – 1s.
- FoV – 400mm.
- Reconstruction kernel – B20 (soft tissue).

3.3 Simulation

The simulation was done using MATLAB R2015b software. The algorithm for the simulation is comprised of two parts:

- Reference noise sample generation and plotting of size/exposure dependence curve from phantom scans.
- Simulation of patient images, using the extracted noise sample data, modifying and combining it with patient scan data.

Reference noise sample generation was done using two independent scans of the same phantom, using the same CT settings. The individual image matrices from the same scan depth were subtracted from one another and the resulting matrix was divided by $\sqrt{2}$ to eliminate sample

bias. These extracted noise samples, representing the noise level at specific tube currents, were modified and then later added to the patient's original image matrix during the simulation. This is possible due to the additivity property of variance.

After acquiring noise samples from all scanned exposure levels, the simulation was performed.

3.4 Image evaluation

All image sets were evaluated on the workstation of the same CT scanner, by a radiologist. Radiologist was allowed to use all the tools available on the workstation, such as changing window width and level, various 3D reconstructions. The evaluations were made 10 at a time, to reduce learning bias. Evaluations were made using the following scale:

1 - Poor visibility/difficult or impossible
to evaluate

2 - Acceptable visibility/evaluation possible

3 - Good visibility/clear evaluation

Table 3. Image evaluation scale

	Case1	Case2
Axial evaluation		
Angle measurement and evaluation		
Reduction procedure control evaluation		
Sharpness/visibility of acetabulum bone edges		
Sharpness of the femoral bone edge		
3D reconstruction evaluation		
Evaluation and visibility of the femoral bone position relative to acetabulum		
Angle measurement and evaluation		

The evaluation criteria were selected, after questioning 4 doctors, related to the diagnosis, evaluation and treatment of the DDH.

Evaluated image sets were then sorted into two outcome groups:

- Evaluation of 1 – Negative.
- Evaluation of 2 or 3 – Positive.

Data analysis was performed using "Microsoft EXCEL 2016" and "SPSS 2014" software.

4. RESULTS

Firstly, the gelatin based phantom was scanned in order to produce the noise samples for every mAs parameters – 13, 20, 50 – that were used for simulation.

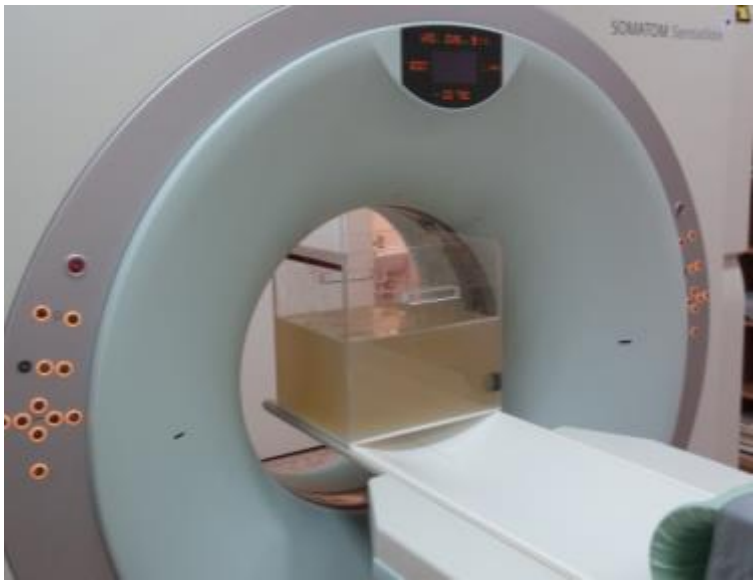

Fig. 13. The phantom position in the scanner

3 scans were made at each exposure level, using parameters described in the methods and materials section, each producing a set of 400 images.

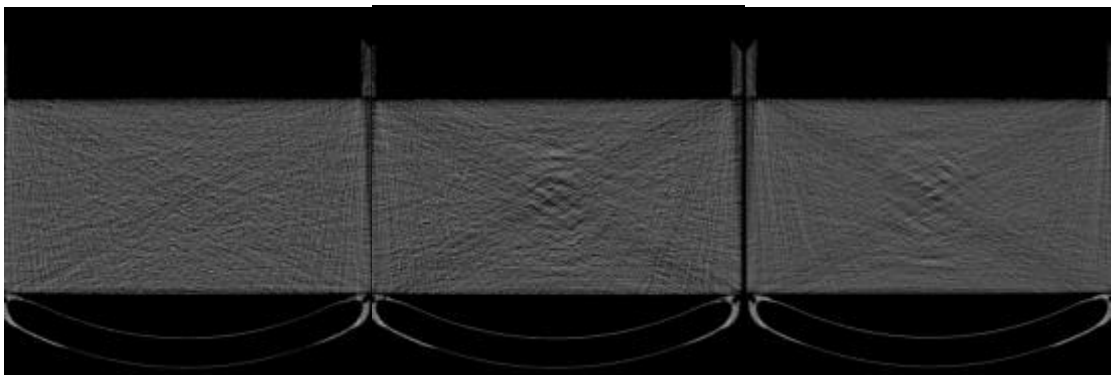

Fig. 14. Examples of phantom scan images at 13, 20 and 50 mAs

Using the images from the gelatin phantom scans, reference noise samples for each of the exposures were produced:

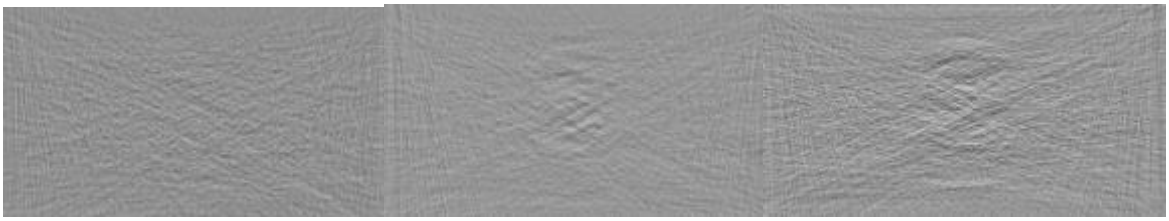

Fig. 15. Noise samples at different exposures – 13,20 and 50 mAs

From both the scans and the noise sample, we can observe distinct cross shaped artifacts, that most likely have been caused by beam hardening induced photon starvation effect, due to the phantom size. It was expected, and since similar artifacts were observed in the actual original patient images, this was done on purpose, when designing the phantom.

After the production of the noise sample, another spherical phantom was scanned, in order to produce the noise-size dependence curves.

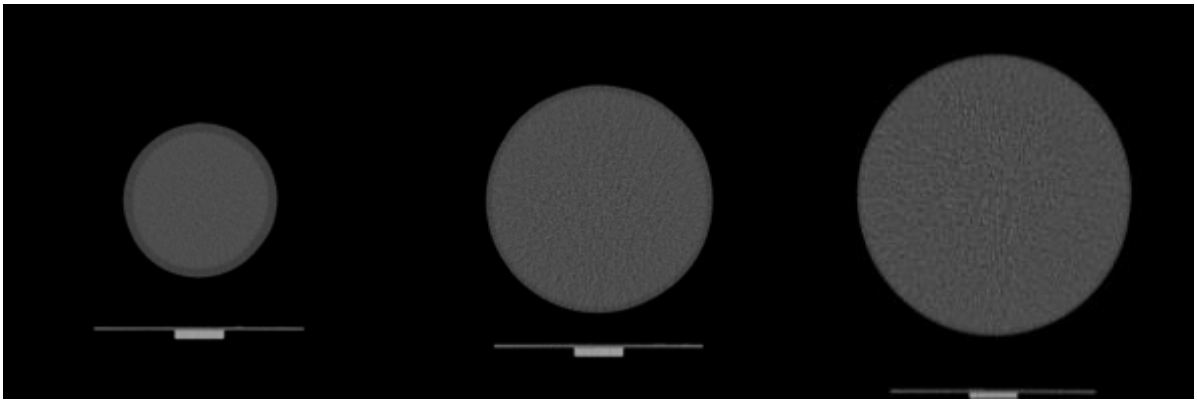

Fig. 16. Slices from the spherical phantom scan representing different size objects

Using MATLAB software, pixel size and then – the area of the circle was calculated. In order to evaluate the noise level, the standard deviation of the pixel values was measured in the center of the circle. These measurements were performed using different slices, where the size and area of the phantom was different. The main size depending curves were derived from these measurements and used in the simulation.

Standard deviation from 178 images of each scan were measured, and their curves plotted:

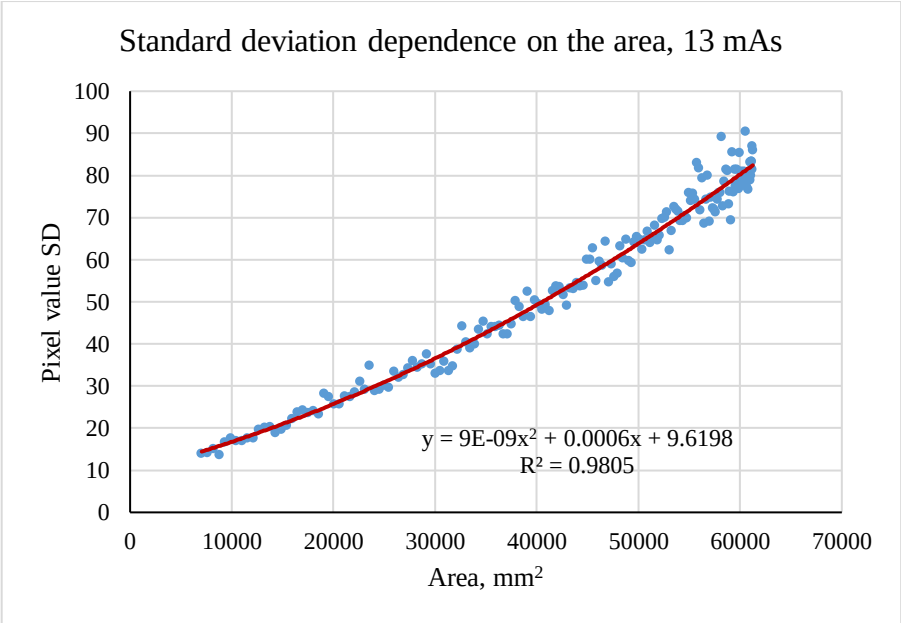

Fig. 17. Size-noise dependence curve at 13 mAs

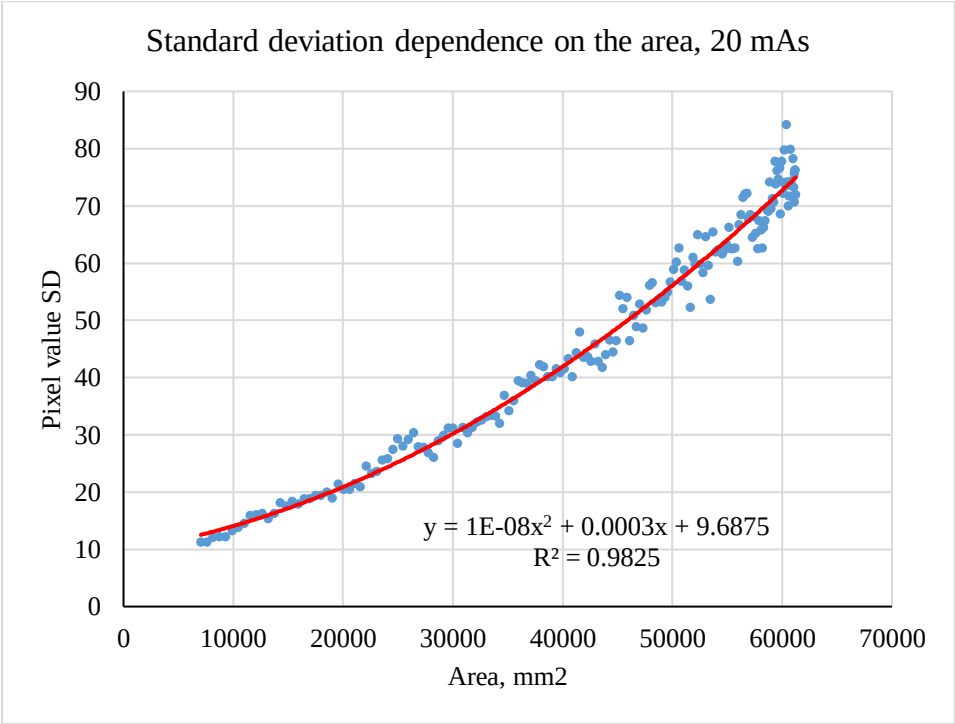

Fig. 18. Size-noise dependence curve at 20 mAs

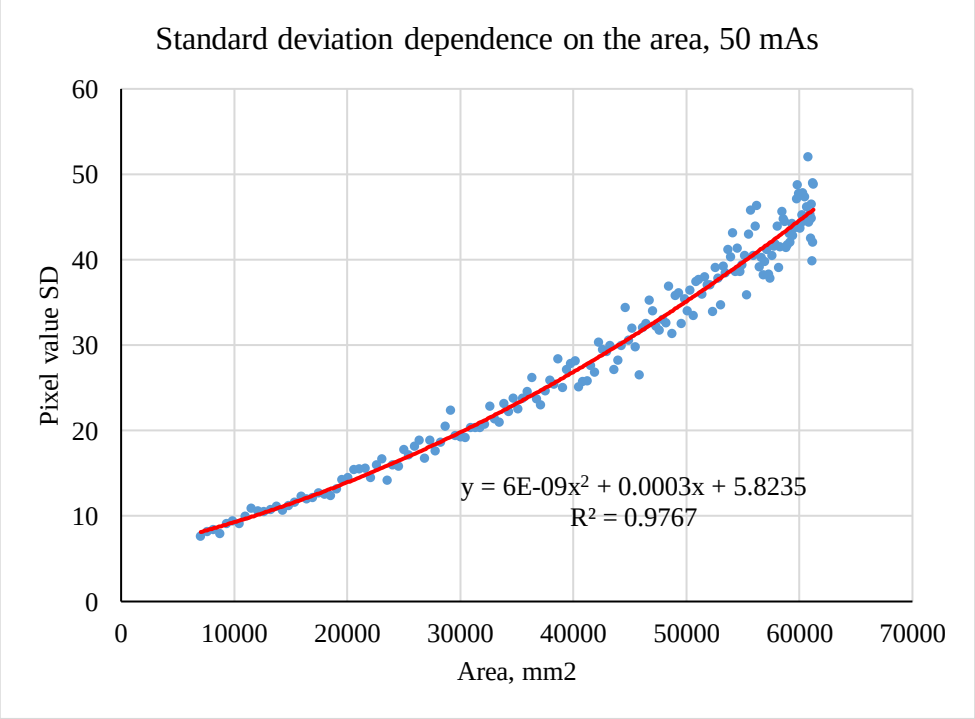

Fig. 19. Size-noise dependence curve at 50 mAs

By using these plots, and by knowing the size of the patient's body in the image, we can approximate the noise level (standard deviation) that should be present in the image. However, since the exposure is different at each slice, depending on the thickness of the patient, the standard deviation needs to be corrected for the specific mAs that was used for the obtaining each image. The relationship, between the noise/standard deviation and mAs, is well described in

literature. After comparing noise levels from scans at different exposures at the same scan depth it was found that the experimental results matched the theory.

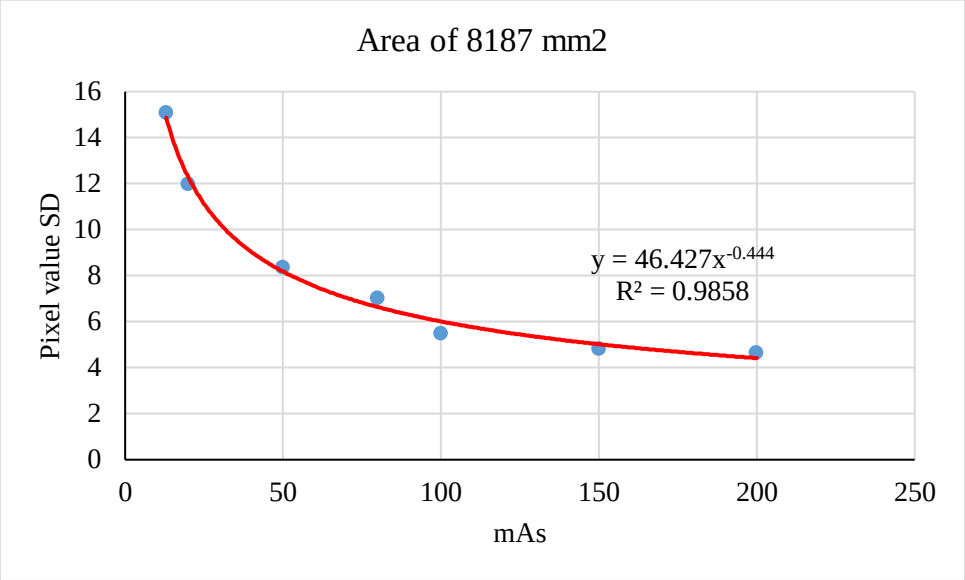

Fig. 20. Noise-mAs relationship of a small area

Experimental results have shown, that the relationship between noise and mAs was the same and does not change at different sizes. Therefore, theoretical relationship between noise and mAs applies and was used in the simulations.

For evaluation of effect of plaster casting on the noise, half of the spherical phantom was wrapped in plaster, using the same technique that is used when immobilizing children after the reduction of DDH. Then phantom was scanned at various mAs. In order to determine, whether plaster cast has any relevant influence on the overall image noise standard deviation was measured.

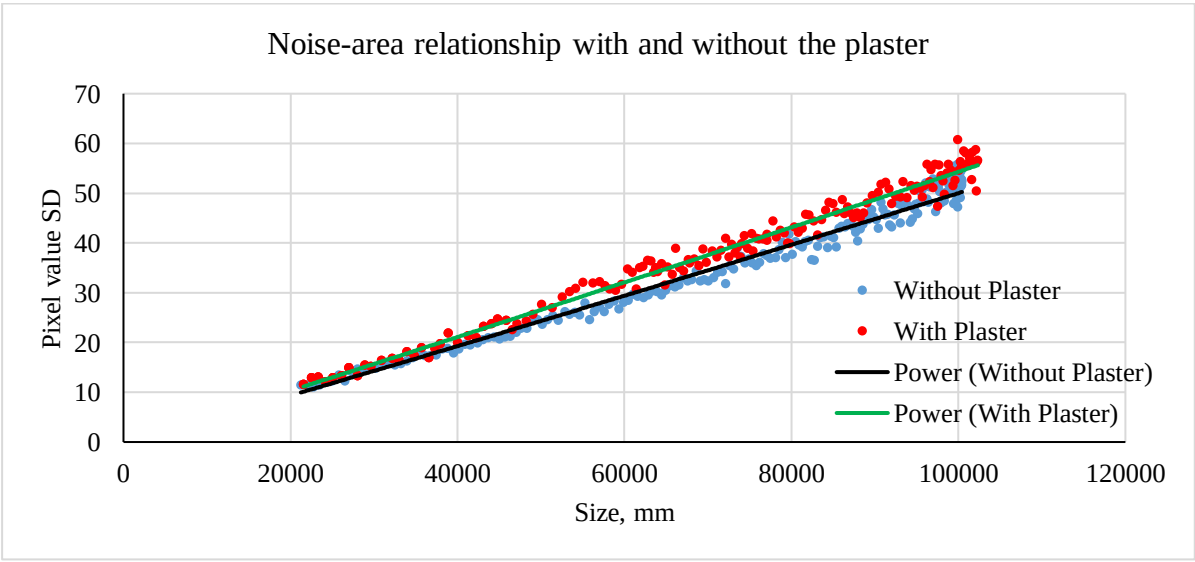

Fig. 21. Noise-area relationship with and without the plaster

After reviewing and analyzing the data from scans at various exposure levels, the influence of plaster on image noise/standard deviation was found to be not significant ($p<0.05$), therefore it was decided not to include it into the final simulation calculations.

After obtaining all the necessary data needed for the simulation, the algorithm was constructed. It consisted of 8 steps:

1. Reading of the image.
2. Filtering and measuring the size of the object in the image (the body of the patient).
    - Size is an important factor in the amount of noise an object produces. Because of this, it is important to know the size (area) of an object occupying the image space. However, due to different size FOV's in the patient files, there were images, in which parts of the patient legs were outside the image space, meanwhile the x-rays have passed the whole leg, regardless of FOV, and therefore the amount of noise present in the image had to be adjusted. Therefore, the problem was determining the correct size of the object, so an elliptical shape approximation for the "outside of image" area was applied, for every image where this occurred.

      Finally, the number of pixels, that the object (patient body) was comprised of, is converted into the area of the object in mm^2.
3. From the area of the object we approximate the amount of noise, that the object of this size would produce. This is done by an approximation curve derived from experimental data, collected using scans of the spherical phantom. By measuring the noise amount in different depths of the spherical phantom, we get the relationship between the object size/area in the image and the noise that it produces at specific exposure levels. Then, by using this relationship we can establish the amount of noise that a patient with the same amount of area would produce at specific exposures – $SD_{simulated}$. From this value, on the basis of theoretical approximation of noise and experimental data, we can determine the amount of noise this patient would have at a higher exposure.

$$SD_{patient} = SD_{simulated} * \frac{1}{\sqrt{\frac{Exposure_{sim}}{Exposure_{actual}}}}; \quad (15)$$

   From this we can approximate the amount of noise that the patient should have in the base image.
4. Determining the noise level for the modified noise sample which will be added to the patient image. If we say, that the simulated image of the patient at the simulated exposure will need to have the amount of noise of $SD_{simulated}$, this value needs to be equal to the

sum of the amount of noise in the patient image and the noise sample. Since these values are the standard deviations of the image, according to the principle of additivity of variances, we get that:

$$(SD_{patient})^2+(SD_{sample})^2 = (SD_{simulated})^2; \quad (16)$$

From equation 16, we can calculate for SD_{sample}, which is:

$$SD_{sample} = \sqrt{(SD_{simulated})^2 - (SD_{patient})^2}; \quad (17)$$

5. Reading the generated noise sample and modifying it. In this step, first we determine the noise in the noise sample image matrix. This is done by measuring the standard deviation in the center. This gives us the amount of the noise present in our generated noise sample – $SD_{gensample}$. Then, we calculate the coefficient k, which is the ratio of the noise of the original generated sample – $SD_{gensample}$, and the calculated SD_{sample}, needed for the simulation

$$k = \frac{SD_{gensample}}{SD_{sample}}; \quad (18)$$

By dividing our generated noise sample matrix by k, we get the needed noise sample matrix, with the standard distribution of SD_{sample}.

6. Shifting the noise sample matrix, so that the main object in the patient image is covered by the whole size of the noise sample.
7. Patient information redaction. In this step the information such as the name, birth date and other information related to the scanning parameters is replaced by placeholders which are known to the data collector and unknown to the reviewing radiologists.
8. In the final step, the modified noise sample matrix is combined with the patient image matrix and the final image is exported.

Using the simulation algorithm described above, image sets for each of the 20 patients were created, adapting the algorithm for each one. For every patient, 3 sets of images with a different exposure parameter were simulated – at 13, 20 and 50 mAs. Figure 23 represents the image that was scanned using a large field of view.

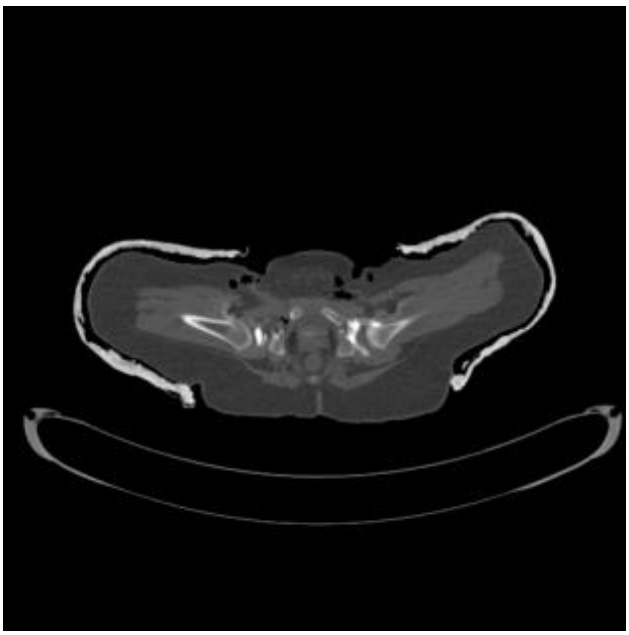

Fig. 22. Original image example, scanned using 100 mAs

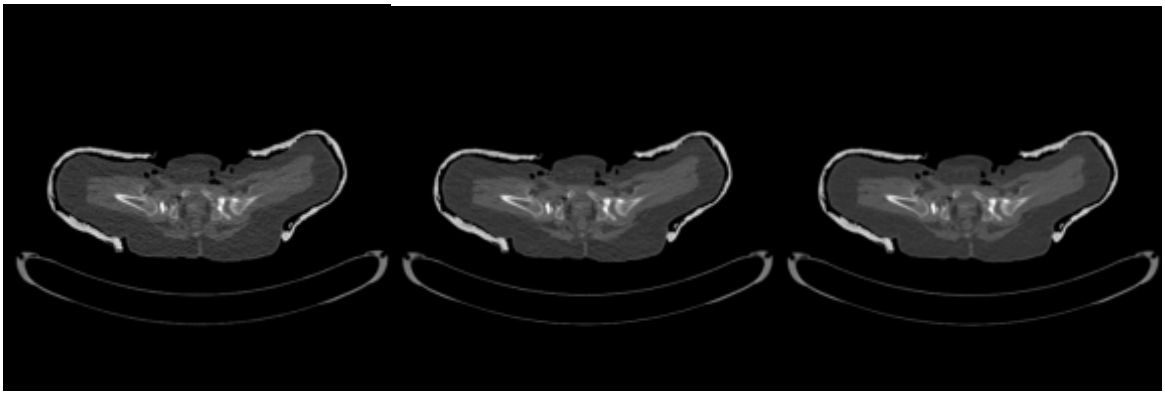

Fig. 23. Simulated images at 13 mAs (left), 20 mAs (center) and 50 mAs (right)

However, most of the images were scanned using smaller fields of view, where part of the body is outside of image space:

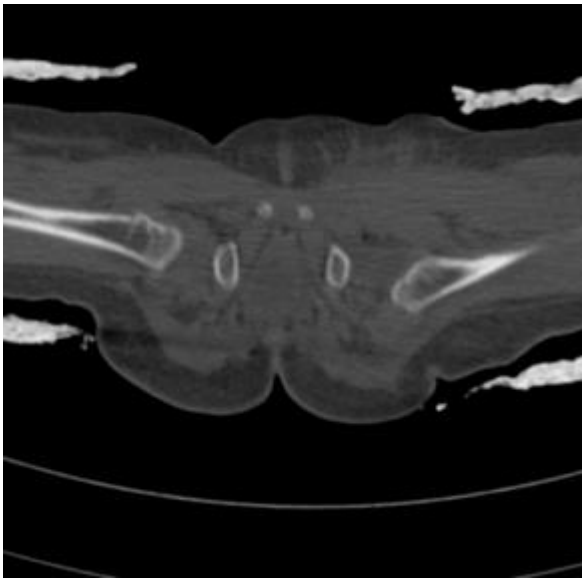

Fig. 24. Original image scanned using 150 mAs

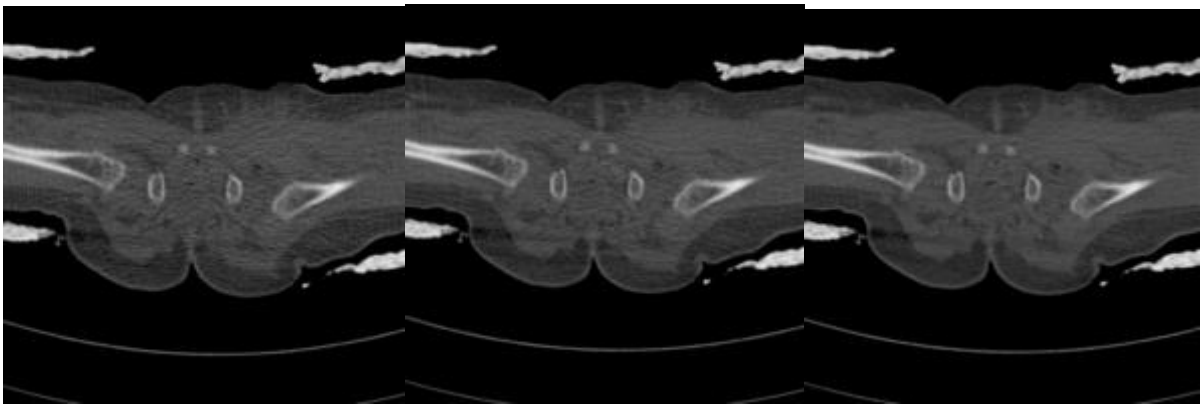

Fig. 25. Simulated images at 13 mAs (left), 20 mAs (center) and 50 mAs (right)

The validation of whether or not the simulation was successful, was made using manual comparisons between the measured SD of various areas on the patient and the measured SD of the spherical phantom with the same area. Since our goal was that the simulated images had the same noise as the ones from the object of the same size in our spherical phantom scans.

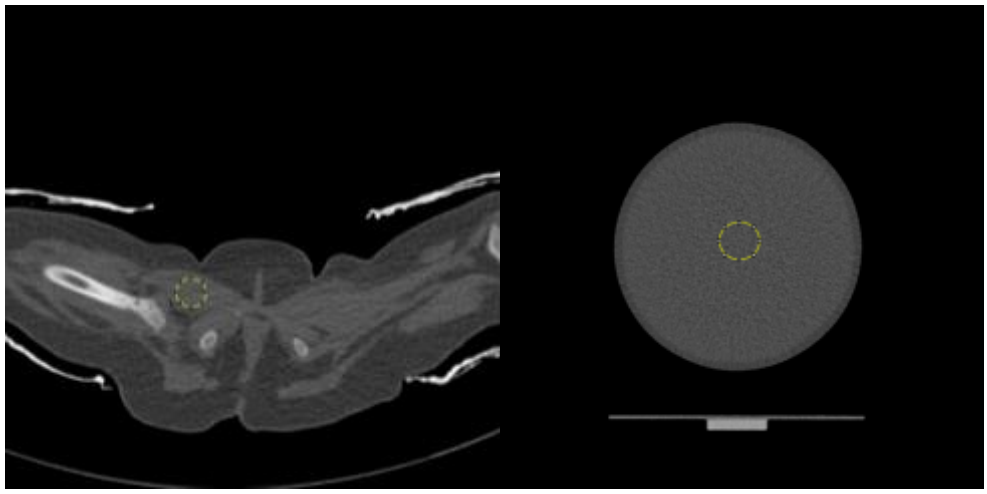

Fig. 26. Comparison of noise between the phantom and simulated images

In the figure 27, on the left side we have the simulated patient image at 13 mAs and on the right – the spherical phantom scan at 13 mAs with the same area as the patient. The SD of the phantom was 40.383 and the SD of the simulated image, at various ROI's that were measured, was 41.231±0.843.

After evaluating the images, using the provided evaluation scale (see table 2), the radiologist determined which of the simulated image sets had acceptable image quality in order to make a reliable evaluation of DDH postreduction control. Out of 60 sets of images, with 3 different mAs simulations (20 each), the following results were sorted into positive and negative outcomes.
Evaluation results when scanning at 50 mAs:

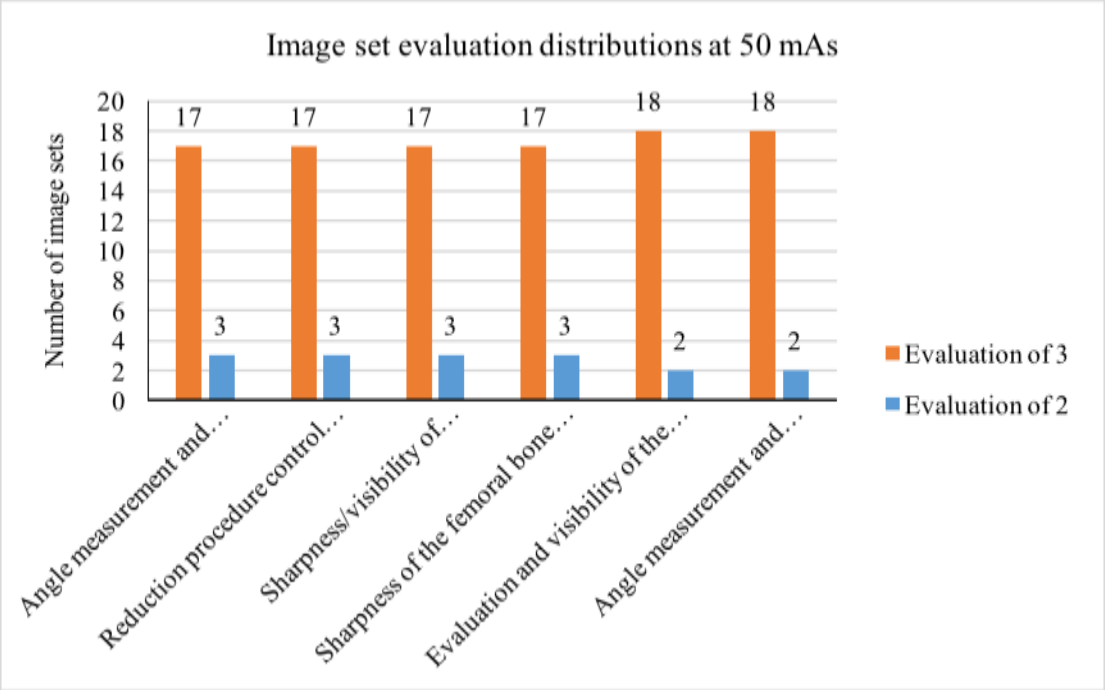

Fig. 27. Evaluation distribution at 50 mAs

After evaluating the simulated image sets at 50 mAs, there were no negative evaluations (1) made. All the images passed, out of which, on average, 88.6% were considered to be of good quality (evaluation 3), and 11.4% were deemed acceptable (evaluation 2), for possible diagnostic evaluation.

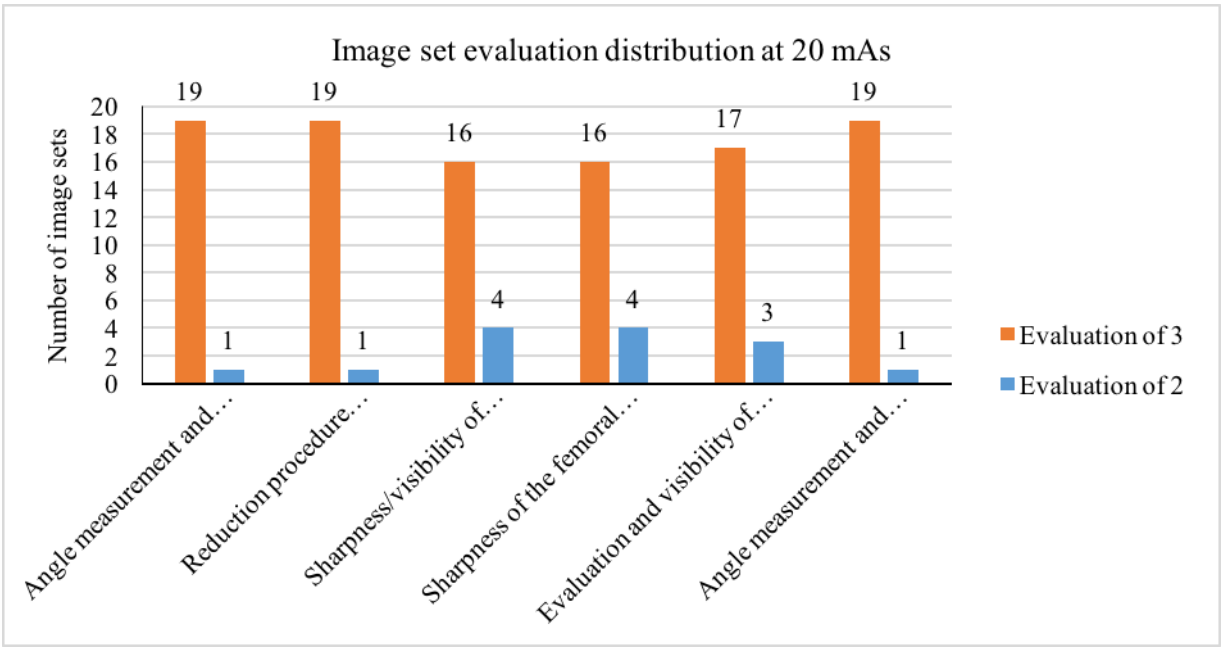

Fig. 28. Evaluation distribution at 20 mAs

In the figure 29 we can see the evaluations for the 20 mAs simulated image sets. As was the case with 50 mAs simulations, there were no negative evaluations. On average 88,33% of the image sets were evaluated as good quality, while 11,66% were considered acceptable.

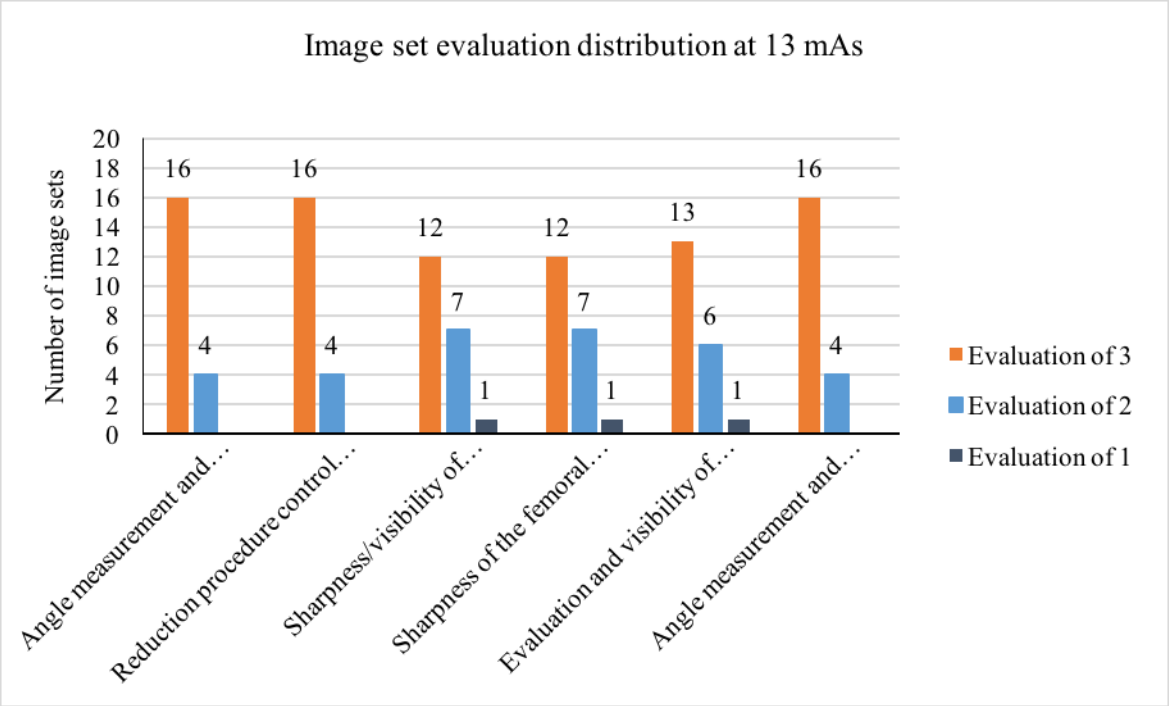

Fig. 29. Evaluation distribution at 13 mAs

In the figure 29, we can observe that there were a few negative evaluations, of the simulations at 13 mAs. On average 70,83% of the image sets were evaluated as good quality, while 26,66% were considered acceptable.

From the evaluation data, the only negative outcomes were detected at 13 mAs. From the feedback of the radiologist, almost all of the images that were rated as acceptable (2), were similar to the ones that were rated better (3), however to achieve the necessary precision for diagnostic evaluation, manipulation of the window settings was usually required.

All in all, the general conclusion would be, that it is possible to reduce the CT scanning parameters. Current scanning protocols, provide high quality images, however this is not necessary for the evaluation and control of DDH case. The successful diagnosis can be achieved using manually selected, much lower mAs settings. This, in turn, would reduce the dose quite significantly, proportionally to mAs used.

If the scans on these patients would have been performed using the mAs values that were used for the simulation, the average patient dose would be lower (Table 4).

Table 4. Decrease in patient dose by factor

	50 mAs	20 mAs	13 mAs
Average reduction	1.7	4.3	6.7
Standard Deviation	1	2.5	3.8
Min	0.7	1.8	2.8
Max	4.4	11.1	17

Another very important part of optimization that was noticed during analysis of patient data – there is no clear preset for the length of the scan. In almost all cases of scanned patients, the scan length far exceeded the anatomical region that is relevant to the diagnosis of DDH.

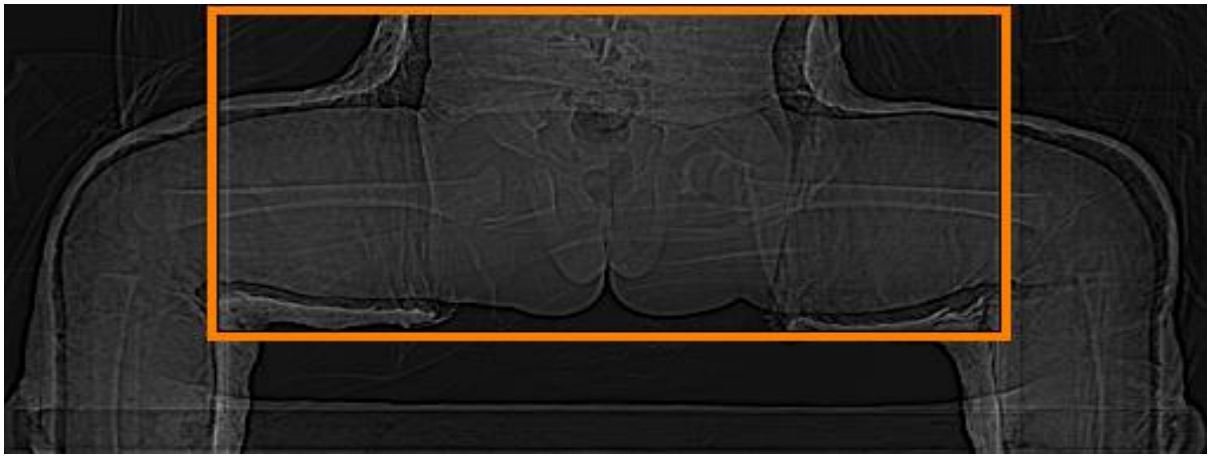

Fig. 30. Typical patient scan length – box width = rFOV, height – scan length

In Figure 31 we can see the usual set for the patient scan. Considering that the relevant information for diagnostic purposes is located only in the hip part of the pelvis, the patient gets an unnecessary dose when a larger scan length, involving the abdomen and lower parts of the legs. This should be coordinated between the technologist, doing the scan and the radiologist.

Therefore, the proposed recommendation for an optimized CT protocol, for postreduction control of the developmental dysplasia of the hip, should be:

- Tube voltage – 120 kV (any lower would increase beam hardening artifacts).
- Manual mAs setting – 13 mAs.
- Reconstruction – Soft tissue filter (B20 in our case).
- Area of the scan (scan length) – only the relevant anatomical part of the pelvis, where the diagnosis is being made.

5. CONCLUSIONS

1. It was found that a specially constructed gelatin phantom was suitable for the phantom based simulation in the case of developmental dysplasia of the hip.
2. Analysis of the factors, that influence the noise in computed tomography images, has shown that the developed noise simulation algorithm was suitable for image noise simulation in the case of developmental dysplasia of the hip
3. By reducing the exposure to 13 mAs, it is still possible to perform successful clinical diagnosis and achieve good postreduction control of developmental dysplasia of the hip.
4. Based on the evaluation results, the recommended CT protocol would effectively reduce the dose and the risk of cancer to the patient, in our case, on average, by a factor of 6.7±3.8.

6. LIST OF REFERENCES

1. PATON, R. W., et al. Developmental dysplasia of the hip (DDH): diagnosis and treatment. *Orthopaedics and Trauma*. 2016, 6(30), p. 453-460.
2. GRISSOM, L., HARCKE, H.T., THACKER, M. Imaging in the Surgical Management of Developmental Dislocation of the Hip. *Clin Orthop Relat Res*. 2008, 466, p. 791-801.
3. MATRAWY, K.A., NOUH, M.R. Ultrasound screening for developmental dysplasia of the hip and its socioeconomic impact: Experience of tertiary care health level. *Alexandria Journal of Medicine*. 2014, 1(50), p. 25-29.
4. BELTRAN, L.S., ROSENBERG Z.S., MAYO, J.D. Imaging Evaluation of Developmental Hip Dysplasia in the Young Adult. *American Journal of Roentgenology*. 2013, 200, p. 1077-1088.
5. SHALABY, M.H., SAMIR, S. CT measurement of femoral anteversion angle in patients with unilateral developmental hip dysplasia: A comparative study between 2D and 3D techniques. *The Egyptian Journal of Radiology and Nuclear Medicine*. 2017.
6. FOX, S.H., TOTH, T. Dose reduction on GE CT scanners. *Pediatric Radiology*. 2002, 32(10), p. 718–723.
7. DE MAN, B., BASUA, S., et al. CATSIM: a new Computer Assisted Tomography SIMulation environment. *Physics of Medical Imaging*. 2007.
8. ZENG, D., HUANG, J., et al. A Simple Low-Dose X-Ray CT Simulation From High-Dose Scan. *IEEE Transactions on Nuclear Science.* 2015, 62(5), p. 226-233.
9. JOEMAI R., GELEIJNS J., VELDKAMP, H. Development and validation of a low dose simulator for computed tomography. *Eur Radiol.* 2010, 20, p. 958–966.
10. BENSON, T. M., BRUNO K., DE MAN, B. Synthetic CT noise emulation in the raw data domain. *IEEE Nuclear Science Symposuim & Medical Imaging Conference*. 2010, p. 3169-3171.
11. KIM, C.W., KIM, J. H. Application of CT Simulation Technique for Virtual Ultra-Low-Dose Trial in CT Colonography. *Abdominal Imaging*. 2012, LNCS 7601, p. 49–57.
12. YU, L., SHIUNG, M., et al. Development and Validation of a Practical Lower-Dose-Simulation Tool for Optimizing Computed Tomography Scan Protocols. *J Comput Assist Tomogr*. 2012, 36, p. 477-487.
13. ŽABIĆ, S., WANG, S., et al. A low dose simulation tool for CT systems with energy integrating detectors. *Medical Physics*,2013, 40, 031102.
14. WANG, A., PELC, N. Synthetic CT: Simulating low dose single and dual energy protocols from a dual energy scan. *Med. Phys*. 2011, 38, 5551–5562.

15. FEFFERMAN, N.R., BOMSZTYK, E., YIM, A.M., et al. Appendicitis in Children: Low-Dose CT with a Phantom-based Simulation Technique—Initial Observations. *Radiology* 2005, 237, p. 641–646.
16. ROBIËL, N.E., et al. Simulation of scanner-and patient-specific low-dose CT imaging from existing CT images. *Med. Phys.* 2017, 36, p. 12-23.
17. KIM, C. W., KIM, J. H. Realistic simulation of reduced-dose CT with noise modeling and sinogram synthesis using DICOM CT images. *Med. Phys.* 2014, 41(1).
18. GOLDMAN, L. W., Principles of CT: Radiation Dose and Image Quality. *J. Nucl. Med. Technol*. 2007, 35(4), p. 213-225.
19. HUDA, W., METTLER, F.A. Volume CT Dose Index and Dose-Length Product Displayed during CT: What Good Are They. *Radiology.* 2011, 258(1), p. 236-242.
20. HUDA, W., OGDEN, K.N., KHORASANI, M.R. Converting DLP product to effective dose at CT. *Radiology*. 2008, 248(3), p. 995–1003.
21. SLOVIS, T.L. Children, computed tomography radiation dose, and the As Low As Reasonably Achievable (ALARA) concept. *Pediatrics*. 2003, 112, p. 971–972.
22. Goske, M.J., Applegate, E.K., Boylan, J., et al. The Image Gently Campaign: Working Together to Change Practice. *American Journal of Roentgenology*. 2008, 190, p. 273-274.
23. AAPM REPORT No. 204. Size-specific dose estimates (SSDE) in pediatric and adult body CT examinations. 2011.
24. HUDA, W., MAGILL, D. CT effective dose per dose length product using ICRP 103 weighting factors. *Med Phys.* 2011, 38(3), p. 1261-5.
25. MCCOLLOUGH, C.H., PRIMAK, A.N. Strategies for Reducing Radiation Dose in CT. *Radiol Clin North Am*. 2009, 47(1), p. 27–40.
26. LINTON, O.W., METTLER F.A. National conference on dose reduction in CT, with an emphasis on pediatric patients. *American Journal of Roentgenology*. 2003, 181(2), p. 321–329.
27. MCCOLLOUGH, C.H., ZINK, F.E., KOFLER J., et al. Dose optimization in CT: creation, implementation and clinical acceptance of size-based technique charts. *Radiology*. 2002, p. 225:591.
28. GRASER, A., WINTERSPERGER, B.J., SUESS, C., et al. Dose reduction and image quality in MDCT colonography using tube current modulation. *American Journal of Roentgenology*. 2006, 187(3), p. 695–701.

29. SÖDERBERG, M., GUNNARSSON, M. Automatic exposure control in computed tomography-an evaluation of systems from different manufacturers. *Acta Radiol*. 2010 51(6), p. 625-34.
30. ALMOHIY, H., ALASA, E.M.M., et al. Correct Patient Centering Increases Image Quality without Concomitant Increase of Radiation Dose during Adult Intracranial Computed Tomography. *Journal of Medical Imaging and Radiation Sciences*. 2016, 47(3), p. 235 – 242.
31. ALI KHAWAJA, A., KALRA, M., et al. CT radiation dose and iterative reconstruction techniques. *American Journal of Roentgenology.* 2015, 204(4), p. 384-392.
32. LIU, H.L. Model-based iterative reconstruction: a promising algorithm for today's computed tomography imaging. *Journal of Medical Imaging and Radiation Sciences.* 2014, 45, p. 131-136.
33. GOLDMAN, L.W. Principles of CT and CT Technology. *J. Nucl. Med. Technol*. 2007, 35(3), p. 115-128.
34. AGENCY, I.A. *Diagnostic radiology physics: a handbook for teachers and students.* Vienna: Intl atomic energy agency. 2013.
35. BALEVIČIUS, V. *Taikomoji optika*. Vilnius, 2000.
36. SMITH S.W. *Digital Signal Processing: A Practical Guide for Engineers and Scientists*. 2002.
37. KALENDER, W.A., *Computed tomography: fundamentals, system technology, image quality, applications*. 2nd edn, Publicis corporate, Erlangen, 2005.
38. XIAOUYU, T., EHSAN, S. Accurate assessment and prediction of noise in clinical CT images. Med. Phys. 2016 vol. 43, p. 475-482.
39. BARRET, J.F., KEAT, N. Artifacts in CT: Recognition and Avoidance. *RadioGraphics.* 2004; 24, p. 1679 –1691.